Constraints on the unitarity triangle angle gamma from Dalitz plot analysis of B-0 -> DK+pi(-) decays

Aaij, R.; Beteta, C. Abellan; Adeva, B.; Adinolfi, M.; Affolder, A.; Ajaltouni, Z.; Akar, S.; Albrecht, J.; Alessio, F.; Alexander, M.

Published in:
Physical Review D

DOI:
10.1103/PhysRevD.93.112018

Publication date:
2016

PHYSICAL REVIEW D **93,** 112018 (2016)

Constraints on the unitarity triangle angle γ from Dalitz plot analysis of $B^0 \to DK^+\pi^-$ decays

R. Aaij *et al.*[*]
(LHCb Collaboration)

(Received 11 February 2016; published 30 June 2016)

The first study is presented of CP violation with an amplitude analysis of the Dalitz plot of $B^0 \to DK^+\pi^-$ decays, with $D \to K^+\pi^-$, K^+K^-, and $\pi^+\pi^-$. The analysis is based on a data sample corresponding to 3.0 fb^{-1} of pp collisions collected with the LHCb detector. No significant CP violation effect is seen, and constraints are placed on the angle γ of the unitarity triangle formed from elements of the Cabibbo-Kobayashi-Maskawa quark mixing matrix. Hadronic parameters associated with the $B^0 \to DK^*(892)^0$ decay are determined for the first time. These measurements can be used to improve the sensitivity to γ of existing and future studies of the $B^0 \to DK^*(892)^0$ decay.

DOI: 10.1103/PhysRevD.93.112018

I. INTRODUCTION

One of the most important challenges of physics today is understanding the origin of the matter-antimatter asymmetry of the Universe. Within the Standard Model (SM) of particle physics, the CP symmetry between particles and antiparticles is broken only by the complex phase in the Cabibbo-Kobayashi-Maskawa (CKM) quark mixing matrix [1,2]. An important parameter in the CKM description of the SM flavor structure is $\gamma \equiv \arg[-V_{ud}V_{ub}^*/(V_{cd}V_{cb}^*)]$, one of the three angles of the unitarity triangle formed from CKM matrix elements [3–5]. Since the SM cannot account for the baryon asymmetry of the Universe [6] new sources of CP violation, that would show up as deviations from the SM, are expected. The precise determination of γ is necessary in order to be able to search for such small deviations.

The value of γ can be determined from the CP-violating interference between the two amplitudes in, for example, $B^+ \to DK^+$ and charge-conjugate decays [7–10]. Here D denotes a neutral charm meson reconstructed in a final state accessible to both $\bar{D}^0$ and D^0 decays, that is therefore a superposition of the $\bar{D}^0$ and D^0 states produced through $b \to cW$ and $b \to uW$ transitions (hereafter referred to as V_{cb} and V_{ub} amplitudes). This approach has negligible theoretical uncertainty in the SM [11] but limited data samples are available experimentally.

A similar method based on $B^0 \to DK^+\pi^-$ decays has been proposed [12,13] to help improve the precision. By studying the Dalitz plot (DP) [14] distributions of $\bar{B}^0$ and B^0 decays, interference between different contributions, such as $B^0 \to D_2^*(2460)^-K^+$ and $B^0 \to DK^*(892)^0$ (Feynman diagrams shown in Fig. 1), can be exploited to obtain additional sensitivity compared to the "quasi-two-body" analysis in which only the region of the DP dominated by the $K^*(892)^0$ resonance is selected [15–17]. The method is illustrated in Fig. 2, where the relative amplitudes of the different channels are sketched in the complex plane. The $B^0 \to \bar{D}^0K^{*0}$ (V_{cb}) amplitude is determined, relative to that for $B^0 \to D_2^{*-}K^+$ decays, from analysis of the Dalitz plot with the neutral D meson reconstructed in a favored decay mode such as $\bar{D}^0 \to K^+\pi^-$. The V_{ub} amplitude can then be obtained from the difference in this relative amplitude compared to the V_{cb} only case when the neutral D meson is reconstructed as a CP eigenstate. A nonzero value of γ causes different relative amplitudes for B^0 and $\bar{B}^0$ decays, and hence CP violation. The method allows the determination of γ and the hadronic parameters r_B and δ_B, which are the relative magnitude and strong (i.e. CP-conserving) phase of the V_{ub} and V_{cb} amplitudes for the $B^0 \to DK^{*0}$ decay, with only CP-even D decays required to be reconstructed in addition to the favored decays. This feature, which is in contrast to the method of Refs. [7,8] that requires samples of both CP-even and CP-odd D decays, is important for analysis of data collected at a hadron collider where reconstruction of D meson decays to CP-odd final states such as $K_S^0\pi^0$ is challenging. The Dalitz analysis method also has only a single ambiguity ($\gamma \leftrightarrow \gamma + \pi$, $\delta_B \leftrightarrow \delta_B + \pi$), whereas the method of Refs. [7,8] has an eightfold ambiguity in the determination of γ.

This paper describes the first study of CP violation with a DP analysis of $B^0 \to DK^+\pi^-$ decays, with a sample corresponding to 3.0 fb^{-1} of pp collision data collected with the LHCb detector at center-of-mass energies of 7 and 8 TeV. The inclusion of charge conjugate processes is implied throughout the paper except where discussing asymmetries.

[*]Full author list given at the end of the article.

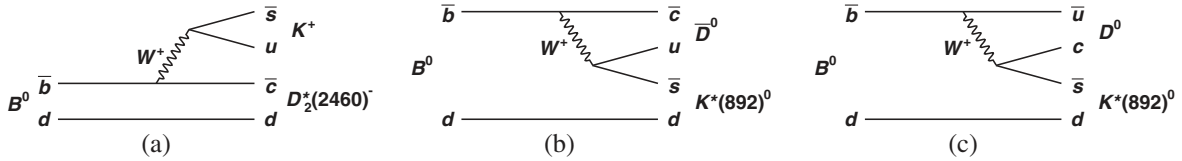

FIG. 1. Feynman diagrams for the contributions to $B^0 \to DK^+\pi^-$ from (a) $B^0 \to D_2^*(2460)^- K^+$, (b) $B^0 \to \bar{D}^0 K^*(892)^0$, and (c) $B^0 \to D^0 K^*(892)^0$ decays.

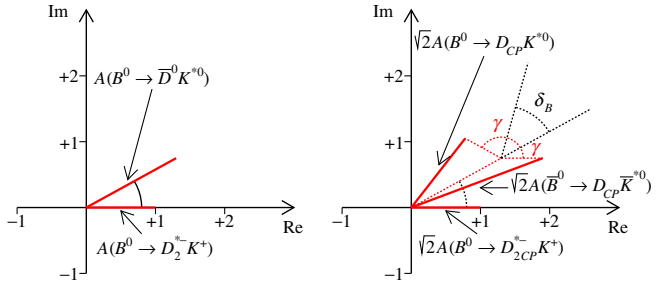

FIG. 2. Illustration of the method to determine γ from Dalitz plot analysis of $B^0 \to DK^+\pi^-$ decays [12,13]: (left) the V_{cb} amplitude for $B^0 \to \bar{D}^0 K^{*0}$ compared to that for $B^0 \to D_2^{*-} K^+$ decay; (right) the effect of the V_{ub} amplitude that contributes to $B^0 \to D_{CP} K^{*0}$ and $\bar{B}^0 \to D_{CP} \bar{K}^{*0}$ decays provides sensitivity to γ. The notation D_{CP} represents a neutral D meson reconstructed in a CP eigenstate, while D_{2CP}^{*-} denotes the decay chain $D_2^{*-} \to D_{CP}\pi^-$, where the charge of the pion tags the flavor of the neutral D meson, independently of the mode in which it is reconstructed, so there is no contribution from the V_{ub} amplitude.

II. DETECTOR AND SIMULATION

The LHCb detector [18,19] is a single-arm forward spectrometer covering the pseudorapidity range $2<\eta<5$, designed for the study of particles containing b or c quarks. The detector includes a high-precision tracking system consisting of a silicon-strip vertex detector surrounding the pp interaction region, a large-area silicon-strip detector located upstream of a dipole magnet with a bending power of about 4 Tm, and three stations of silicon-strip detectors and straw drift tubes placed downstream of the magnet. The tracking system provides a measurement of momentum, p, of charged particles with a relative uncertainty that varies from 0.5% at low momentum to 1.0% at 200 GeV/c. The minimum distance of a track to a primary vertex, the impact parameter, is measured with a resolution of $(15+29/p_{\mathrm{T}})\,\mu$m, where p_{T} is the component of the momentum transverse to the beam, in GeV/c. Different types of charged hadrons are distinguished using information from two ring-imaging Cherenkov detectors. Photons, electrons, and hadrons are identified by a calorimeter system consisting of scintillating-pad and preshower detectors, an electromagnetic calorimeter and a hadronic calorimeter. Muons are identified by a system composed of alternating layers of iron and multiwire proportional chambers. The online event selection is performed by a trigger, which consists of a hardware stage, based on information from the calorimeter and muon systems, followed by a software stage, in which all charged particles with $p_{\mathrm{T}} > 500(300)$ MeV/c are reconstructed for 2011 (2012) data. A detailed description of the trigger conditions is available in Ref. [20].

Simulated data samples are used to study the response of the detector and to investigate certain categories of background. In the simulation, pp collisions are generated using PYTHIA [21] with a specific LHCb configuration [22]. Decays of hadronic particles are described by EVTGEN [23], in which final-state radiation is generated using PHOTOS [24]. The interaction of the generated particles with the detector, and its response, are implemented using the GEANT4 toolkit [25] as described in Ref. [26].

III. SELECTION

Candidate $B^0 \to DK^+\pi^-$ decays are selected with the D meson decaying into the $K^+\pi^-$, K^+K^-, or $\pi^+\pi^-$ final state. The selection requirements are similar to those used for the DP analyses of $B^0 \to \bar{D}^0 K^+\pi^-$ [27] and $B_s^0 \to \bar{D}^0 K^-\pi^+$ [28,29] decays, where in both cases only the $\bar{D}^0 \to K^+\pi^-$ mode was used.

The more copious $B^0 \to D\pi^+\pi^-$ modes, with neutral D meson decays to one of the three final states under study, are used as control channels to optimize the selection requirements. Loose initial requirements on the final state tracks and the D and B candidates are used to obtain a visible peak of $B^0 \to D\pi^+\pi^-$ decays. The neutral D meson candidate must satisfy criteria on its invariant mass, vertex quality, and flight distance from any PV and from the B candidate vertex. Requirements on the outputs of boosted decision tree algorithms that identify neutral D meson decays, in each of the decay chains of interest, originating from b hadron decays [30,31] are also applied. These requirements are sufficient to reduce to negligible levels potential background from charmless B meson decays that

have identical final states but without an intermediate D meson. Vetoes are applied to remove backgrounds from $B^0 \to D^*(2010)^- K^+$, $B^0 \to D^\mp \pi^\pm$, $B_s^0 \to D_s^- \pi^+$, and $B^0_{(s)} \to D^0 \bar{D}^0$ decays, and candidates consistent with originating from $B^0_{(s)} \to \bar{D}^0 K^\pm \pi^\mp$ decays, where the $\bar{D}^0$ has been reconstructed from the wrong pair of tracks.

Separate neural network (NN) classifiers [32] for each D decay mode are used to distinguish signal decays from combinatorial background. The *sPlot* technique [33], with the $B^0 \to D\pi^+\pi^-$ candidate mass as the discriminating variable, is used to obtain signal and background weights, which are then used to train the networks. The networks are based on input variables that describe the topology of each decay channel, and that depend only weakly on the B candidate mass and on the position of the candidate in the B decay Dalitz plot. Loose requirements are made on the NN outputs in order to retain large samples for the DP analysis.

IV. DETERMINATION OF SIGNAL AND BACKGROUND YIELDS

The yields of signal and of several different backgrounds are determined from an extended maximum likelihood fit,

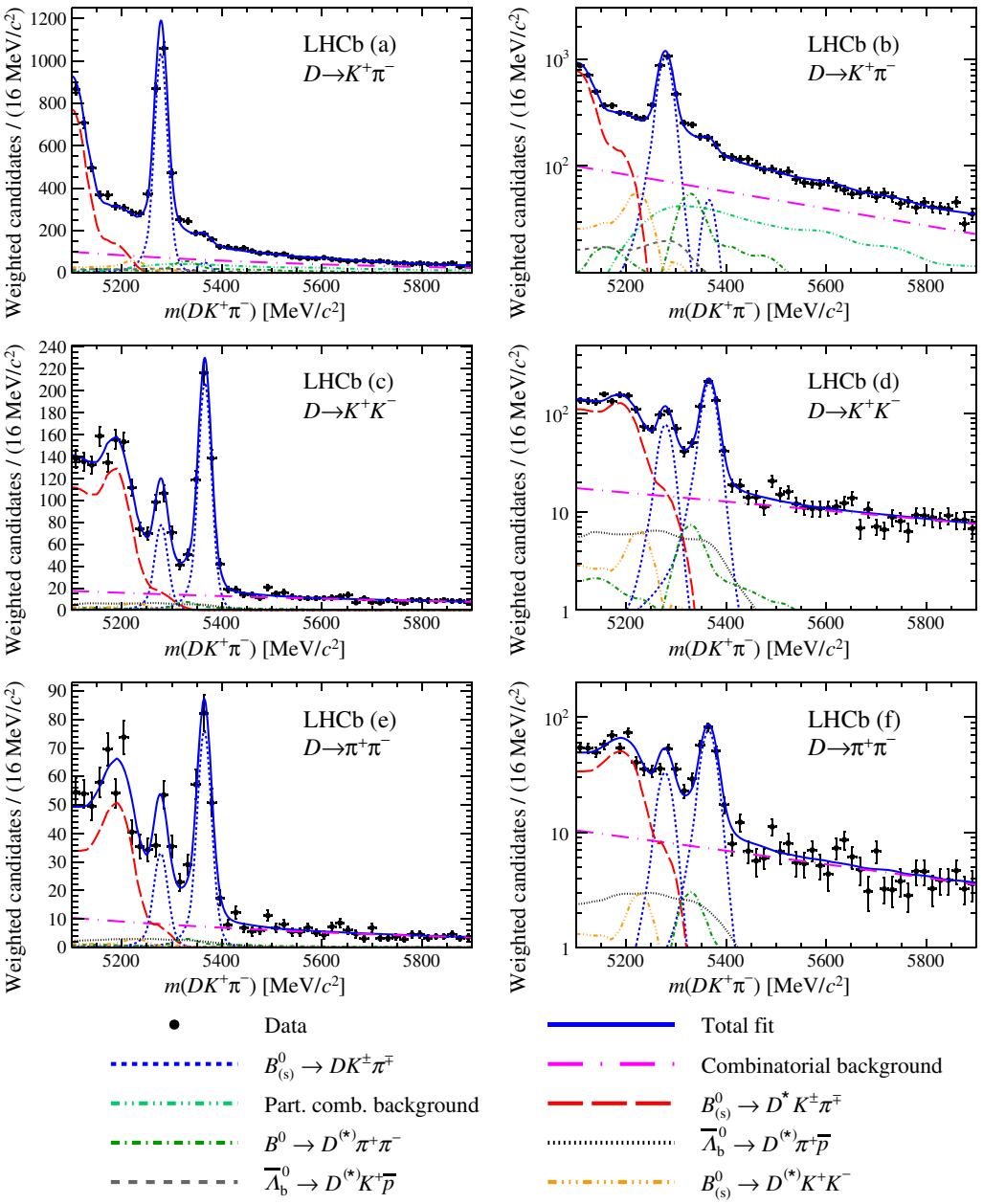

FIG. 3. Results of fits to $DK^+\pi^-$ candidates in the (a,b) $D \to K^+\pi^-$, (c,d) $D \to K^+K^-$, and (e,f) $D \to \pi^+\pi^-$ samples. The data and the fit results in each NN output bin have been weighted according to $\mathcal{S}/(\mathcal{S}+\mathcal{B})$ as described in the text. The left and right plots are identical but with (left) linear and (right) logarithmic y axis scales. The components are as described in the legend.

in each mode, to the distributions of candidates in B candidate mass and NN output. Unbinned information on the B candidate mass is used, while each sample is divided into five bins of the NN output that contain a similar number of signal, and varying numbers of background, decays [34,35].

In addition to $B^0 \to DK^+\pi^-$ decays, components are included in the fit to account for B_s^0 decays to the same final state, partially reconstructed $B^0_{(s)} \to D^{(*)}K^\pm\pi^\mp$ backgrounds, misidentified $B^0 \to D^{(*)}\pi^+\pi^-$, $B^0_{(s)} \to D^{(*)}K^+K^-$, $\bar{\Lambda}_b^0 \to D^{(*)}\bar{p}\pi^+$, and $\bar{\Lambda}_b^0 \to D^{(*)}\bar{p}K^+$ decays as well as combinatorial background. The modeling of the signal and background distributions in B candidate mass is similar to that described in Ref. [27]. The sum of two Crystal Ball functions [36] is used for each of the correctly reconstructed B decays, where the peak position and core width (i.e. the narrower of the two widths) are free parameters of the fit, while the B_s^0–B^0 mass difference is fixed to its known value [37]. The fraction of the signal function contained in the core and the relative width of the two components are constrained within uncertainties to, and all other parameters are fixed to, their expected values obtained from simulated data, separately for each of the three D samples. An exponential function is used to describe combinatorial background, with the shape parameter allowed to vary. Because of the loose NN output requirement it is necessary, in the $D \to K^+\pi^-$ sample, to account explicitly for partially combinatorial background where the final state DK^+ pair originates from a B decay but is combined with a random pion; this is modeled with a nonparametric function. Nonparametric functions obtained from simulation based on known DP distributions [38–44] are used to model the partially reconstructed and misidentified B decays.

The fraction of signal decays in each NN output bin is allowed to vary freely in the fit; the correctly reconstructed B_s^0 decays and misidentified backgrounds are taken to have the same NN output distribution as signal. The fractions of combinatorial and partially reconstructed backgrounds in each NN output bin are each allowed to vary freely. All yields are free parameters of the fit, except those for misidentified backgrounds which are constrained within expectation relative to the signal yield, since the relative branching fractions [37] and misidentification probabilities [45] are well known.

The results of the fits are shown in Fig. 3, in which the NN output bins have been combined by weighting both the data and fit results by $\mathcal{S}/(\mathcal{S}+\mathcal{B})$, where $\mathcal{S}$ ($\mathcal{B}$) is the signal (background) yield in the signal window, defined as $\pm 2.5\sigma$(core) around the B^0 peak in each sample, where σ(core) is the core width of the signal shape. The yields of each category in these regions, which correspond to 5246.6–5309.9 MeV/c^2, 5246.9–5310.5 MeV/c^2, and 5243.1–5312.3 MeV/c^2 in the $D \to K^+\pi^-$, K^+K^-, and

TABLE I. Yields in the signal window of the fit components in the five NN output bins for the $D \to K^+\pi^-$ sample. The last column indicates whether or not each component is explicitly modeled in the Dalitz plot fit.

	Yield					
Component	Bin 1	Bin 2	Bin 3	Bin 4	Bin 5	Included?
$B^0 \to DK^+\pi^-$	597	546	585	571	540	Yes
$B_s^0 \to DK^+\pi^-$	1	1	1	1	1	No
Combinatorial background	540	58	16	6	1	Yes
$B^+ \to D^{(*)}K^+ + X^-$	305	33	9	3	1	Yes
$B^0 \to D^*K^+\pi^-$	1	1	1	1	1	No
$B^0 \to D^{(*)}\pi^+\pi^-$	20	18	20	19	18	Yes
$\bar{\Lambda}_b^0 \to D^{(*)}K^+\bar{p}$	21	19	21	20	19	Yes
$B^0 \to D^{(*)}K^+K^-$	8	7	8	7	7	No
$B_s^0 \to D^{(*)}K^+K^-$	10	9	10	10	9	No

TABLE II. Yields in the signal window of the fit components in the five NN output bins for the $D \to K^+K^-$ sample. The last column indicates whether or not each component is explicitly modeled in the Dalitz plot fit.

	Yield					
Component	Bin 1	Bin 2	Bin 3	Bin 4	Bin 5	Included?
$B^0 \to DK^+\pi^-$	70	63	68	73	65	Yes
$\bar{B}_s^0 \to DK^+\pi^-$	5	5	5	6	5	Yes
Combinatorial background	173	19	9	3	0	Yes
$B^0 \to D^*K^+\pi^-$	0	1	1	1	0	No
$\bar{B}_s^0 \to D^*K^+\pi^-$	19	28	34	28	20	Yes
$B^0 \to D^{(*)}\pi^+\pi^-$	4	3	4	4	3	Yes
$\Lambda_b^0 \to D^{(*)}p\pi^-$	11	10	10	11	10	Yes
$\bar{\Lambda}_b^0 \to D^{(*)}K^+\bar{p}$	2	1	2	2	2	No
$B^0 \to D^{(*)}K^+K^-$	2	1	2	2	1	No
$B_s^0 \to D^{(*)}K^+K^-$	1	1	1	2	1	No

TABLE III. Yields in the signal window of the fit components in the five NN output bins for the $D \to \pi^+\pi^-$ sample. The last column indicates whether or not each component is explicitly modeled in the Dalitz plot fit.

	Yield					
Component	Bin 1	Bin 2	Bin 3	Bin 4	Bin 5	Included?
$B^0 \to DK^+\pi^-$	36	31	38	32	31	Yes
$\bar{B}_s^0 \to DK^+\pi^-$	3	2	3	3	2	Yes
Combinatorial background	119	17	4	3	2	Yes
$B^0 \to D^*K^+\pi^-$	0	0	0	0	0	No
$\bar{B}_s^0 \to D^*K^+\pi^-$	9	16	15	12	10	Yes
$B^0 \to D^{(*)}\pi^+\pi^-$	2	2	2	2	2	Yes
$\Lambda_b^0 \to D^{(*)}p\pi^-$	6	5	6	5	5	Yes
$\bar{\Lambda}_b^0 \to D^{(*)}K^+\bar{p}$	1	1	1	1	1	No
$B^0 \to D^{(*)}K^+K^-$	1	1	1	1	1	No
$B_s^0 \to D^{(*)}K^+K^-$	1	1	1	1	1	No

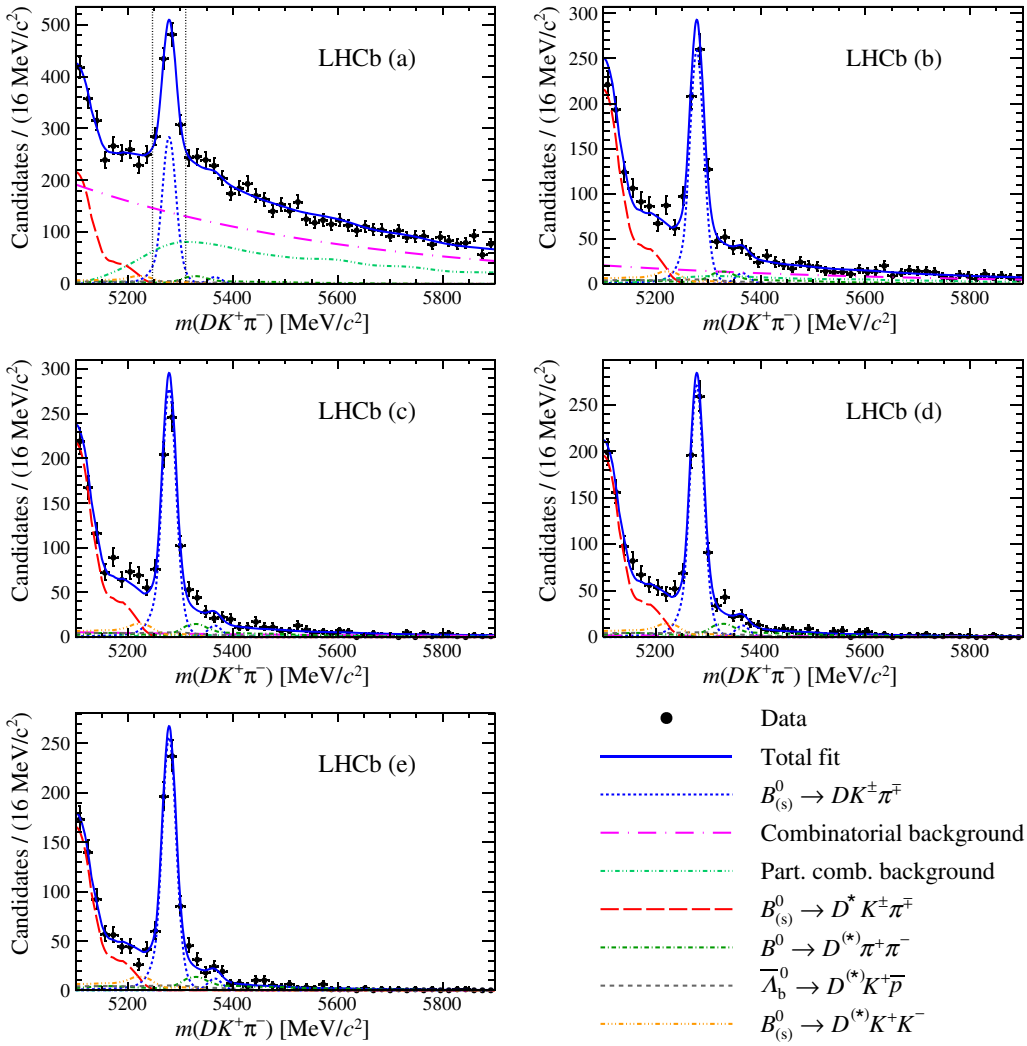

FIG. 4. Results of the fit to $DK^+\pi^-$, $D \to K^+\pi^-$ candidates shown separately in the five bins of the neural network output variable. The bins are shown, from (a)–(e), in order of increasing $\mathcal{S}/\mathcal{B}$. The components are as indicated in the legend. The vertical dotted lines in (a) show the signal window used for the fit to the Dalitz plot.

$\pi^+\pi^-$ samples, are given in Tables I, II and III. In total, there are 2840 ± 70 signal decays within the signal window in the $D \to K^+\pi^-$ sample, while the corresponding values for the $D \to K^+K^-$ and $D \to \pi^+\pi^-$ samples are 339 ± 22 and 168 ± 19. The χ^2/ndf values for the projections of the fits to the $D \to K^+\pi^-$, $D \to K^+K^-$, and $D \to \pi^+\pi^-$ data sets are 171.5/223, 188.2/223, and 169.1/222, respectively, giving a total $\chi^2/\text{ndf} = 528.8/668$. Note that there are some bins with low numbers of entries which may result in this value not following exactly the expected χ^2 distribution.

Projections of the fits separated by NN output bin in each sample are shown in Figs. 4–6. The fitted parameters obtained from all three data samples are reported in Table IV. The parameters $\mu(B)$, $N(\text{core})/N(\text{total})$, $\sigma(\text{wide})/\sigma(\text{core})$ are, respectively, the peak position, the fraction of the signal function contained in the core, and the relative width of the two components of the B^0 signal shape. Quantities denoted N are total yields of each fit component, while those denoted f^i_{signal} are fractions of the signal in NN output bin i (with similar notation for the fractions of the partially reconstructed and combinatorial backgrounds). The NN output bin labels 1–5 range from the bin with the lowest to highest value of $\mathcal{S}/\mathcal{B}$.

V. DALITZ PLOT ANALYSIS

Candidates within the signal region are used in the DP analysis. A simultaneous fit is performed to the samples with different D decays by using the J_{FIT} method [46] as implemented in the Laura++ package [47]. The likelihood function contains signal and background terms, with yields in each NN output bin fixed according to the results obtained previously. The NN output bin with the lowest $\mathcal{S}/\mathcal{B}$ value in the $D \to K^+\pi^-$ sample only is found not to contribute significantly to the sensitivity and is susceptible

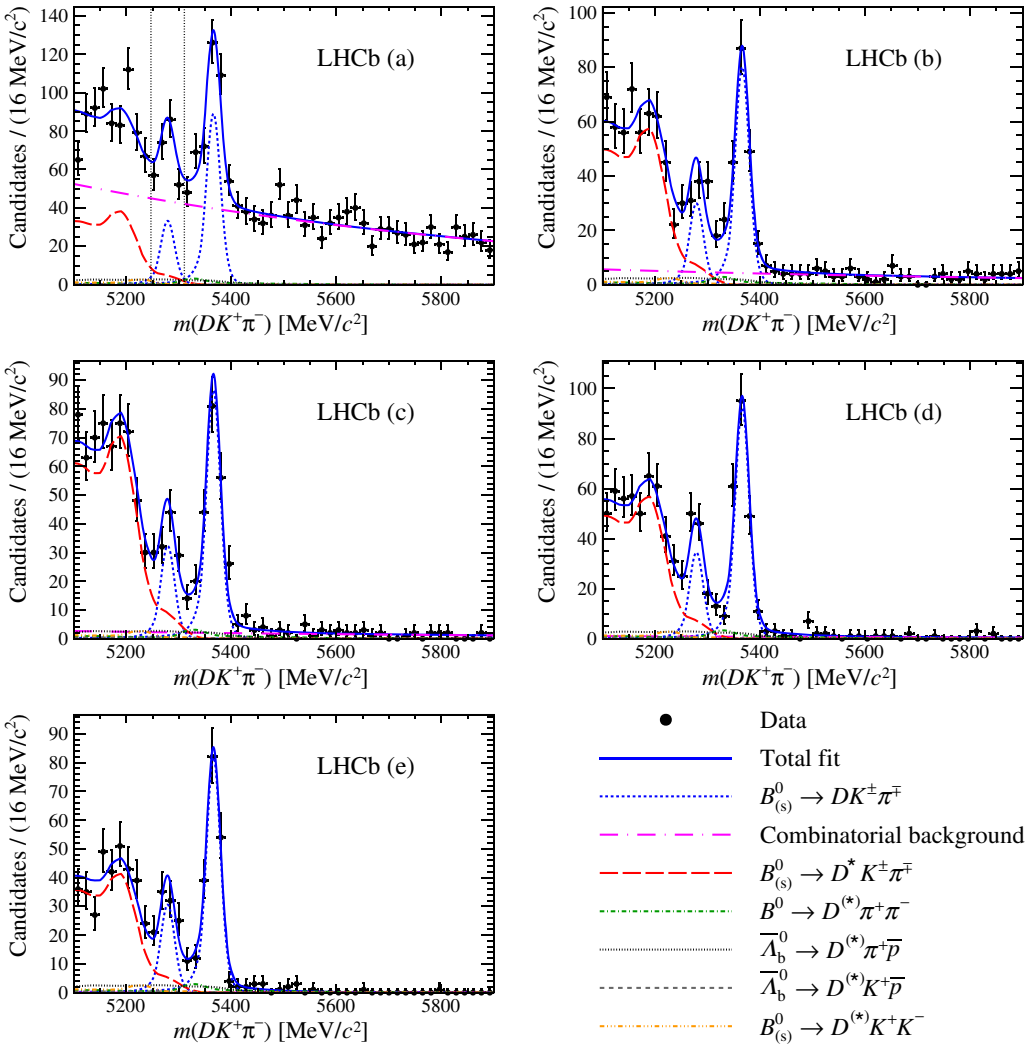

FIG. 5. Results of the fit to $DK^+\pi^-$, $D \to K^+K^-$ candidates shown separately in the five bins of the neural network output variable. The bins are shown, from (a)–(e), in order of increasing $\mathcal{S}/\mathcal{B}$. The components are as indicated in the legend. The vertical dotted lines in (a) show the signal window used for the fit to the Dalitz plot.

to mismodeling of the combinatorial background; it is therefore excluded from the subsequent analysis.

The signal probability function is derived from the isobar model obtained in Ref. [27], with amplitude

$$\mathcal{A}(m^2(D\pi^-), m^2(K^+\pi^-)) = \sum_{j=1}^{N} c_j F_j(m^2(D\pi^-), m^2(K^+\pi^-)), \quad (1)$$

where c_j are complex coefficients describing the relative contribution for each intermediate process, and the $F_j(m^2(D\pi^-), m^2(K^+\pi^-))$ terms describe the resonant dynamics through the line shape, angular distribution, and barrier factors. The sum is over amplitudes from the $D_0^*(2400)^-$, $D_2^*(2460)^-$, $K^*(892)^0$, $K^*(1410)^0$, and $K_2^*(1430)^0$ resonances as well as a $K^+\pi^-$ S-wave component and both S-wave and P-wave nonresonant $D\pi^-$ amplitudes [27]. The masses and widths of $K^+\pi^-$ resonances are fixed, and those of $D\pi^-$ resonances are constrained within uncertainties to known values [27,37,40,48]. The values of the c_j coefficients are allowed to vary in the fit, as are the shape parameters of the nonresonant amplitudes.

For the $D \to K^+\pi^-$ sample, the contribution from the V_{ub} amplitude followed by doubly Cabibbo-suppressed D decay is negligible. This sample can therefore be treated as if only the V_{cb} amplitude contributes, and the signal probability function is given by Eq. (1). For the samples with $D \to K^+K^-$ and $\pi^+\pi^-$ decays, the c_j terms are modified,

$$c_j \to \begin{cases} c_j & \text{for a } D\pi^- \text{ resonance,} \\ c_j[1 + x_{\pm,j} + iy_{\pm,j}] & \text{for a } K^+\pi^- \text{resonance,} \end{cases} \quad (2)$$

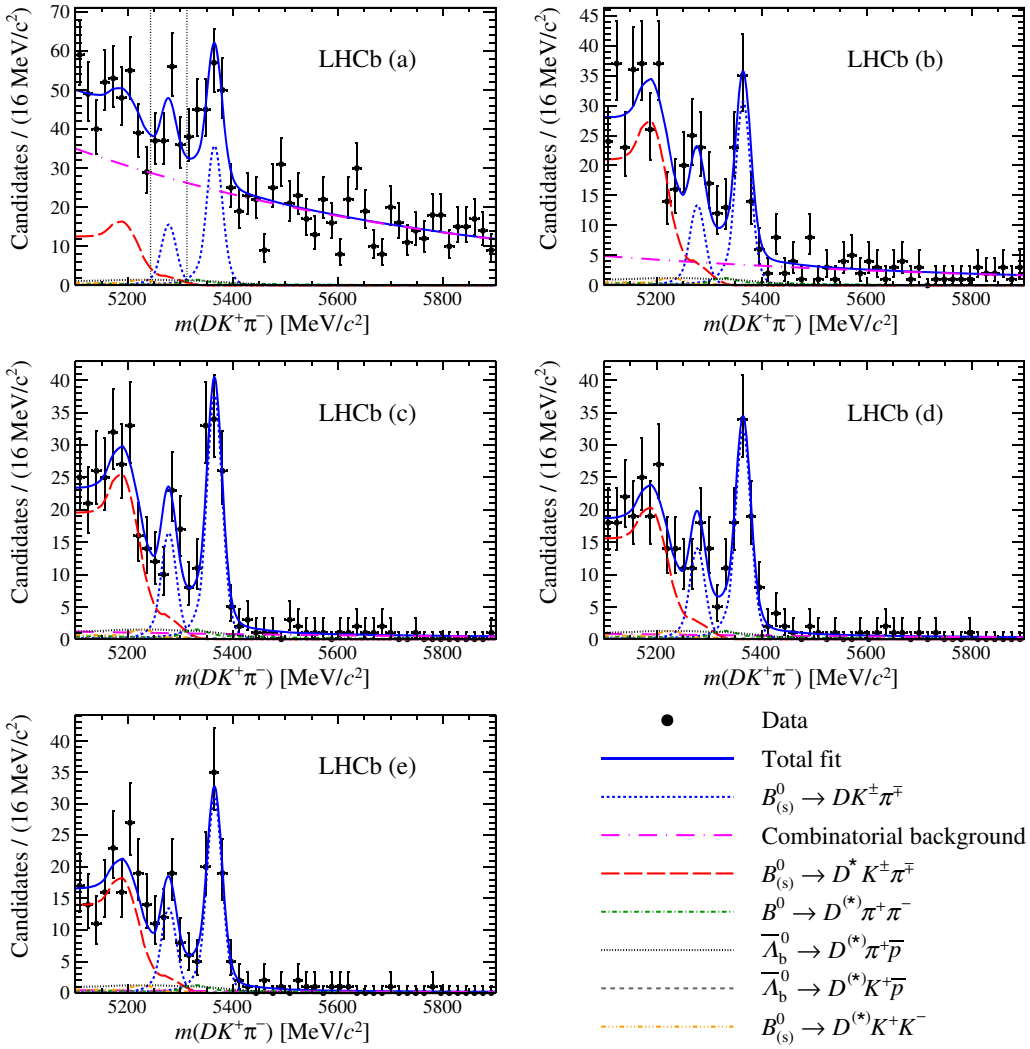

FIG. 6. Results of the fit to $DK^+\pi^-$, $D \to \pi^+\pi^-$ candidates shown separately in the five bins of the neural network output variable. The bins are shown, from (a)–(e), in order of increasing $\mathcal{S}/\mathcal{B}$. The components are as indicated in the legend. The vertical dotted lines in (a) show the signal window used for the fit to the Dalitz plot.

with $x_{\pm,j} = r_{B,j}\cos(\delta_{B,j} \pm \gamma)$ and $y_{\pm,j} = r_{B,j}\sin(\delta_{B,j} \pm \gamma)$, where the $+$ and $-$ signs correspond to B^0 and $\bar{B}^0$ DPs, respectively. Here $r_{B,j}$ and $\delta_{B,j}$ are the relative magnitude and strong phase of the V_{ub} and V_{cb} amplitudes for each $K^+\pi^-$ resonance j. In this analysis the $x_{\pm,j}$ and $y_{\pm,j}$ parameters are measured only for the $K^*(892)^0$ resonance, which has a large enough yield and a sufficiently well-understood line shape to allow reliable determinations of these parameters; therefore the j subscript is omitted hereafter. In addition, a component corresponding to the $B^0 \to D^*_{s1}(2700)^+\pi^-$ decay, which is mediated by the V_{ub} amplitude alone, is included in the fit with mass and width parameters fixed to their known values [37,49] and magnitude constrained according to expectation based on the $B^0 \to D^*_{s1}(2700)^+D^-$ decay rate [49].

The signal efficiency and backgrounds are modeled in the likelihood function, separately for each of the samples, following Refs. [27,38,39]. The DP distribution of combinatorial background is obtained from a sideband in B candidate mass, defined as $5400(5450) < m(DK^+\pi^-) < 5900\ \mathrm{MeV}/c^2$ for the samples with $D \to K^+\pi^-$ ($D \to K^+K^-$ or $\pi^+\pi^-$). The shapes of partially reconstructed and misidentified backgrounds are obtained from simulated samples based on known DP distributions [38–44]. Combinatorial background is the largest component in the NN output bins with the lowest $\mathcal{S}/\mathcal{B}$ values, while in the purest bins in the $D \to K^+K^-$ and $\pi^+\pi^-$ samples the $B^0_s \to D^*K^-\pi^+$ background makes an important contribution. Background sources with yields below 2% relative to the signal in all NN bins are neglected, as indicated in Tables I, II and III.

The fit procedure is validated with ensembles of pseudoexperiments. In addition, samples of $B^0_s \to DK^-\pi^+$ decays are selected for each of the D decays. These are used to test the fit with a model based on that of Refs. [38,39] and where DK^- resonances have contributions only from

TABLE IV. Results for the unconstrained parameters obtained from the fits to the three data samples. Entries where no number is given are fixed to zero. Fractions marked $*$ are not varied in the fit, and give the difference between unity and the sum of the other fractions.

	$D \to K^+\pi^-$	$D \to K^+K^-$	$D \to \pi^+\pi^-$
Parameter		Value	
$\mu(B)(\mathrm{MeV}/c^2)$	5278.3 ± 0.4	5278.7 ± 0.5	5277.7 ± 1.0
$\sigma(\mathrm{core})(\mathrm{MeV}/c^2)$	12.7 ± 0.4	12.7 ± 0.5	13.9 ± 0.8
$N(\mathrm{core})/N(\mathrm{total})$	0.787 ± 0.017	0.798 ± 0.018	0.797 ± 0.018
$\sigma(\mathrm{wide})/\sigma(\mathrm{core})$	1.80 ± 0.05	1.75 ± 0.05	1.76 ± 0.05
Exp. slope (c^2/GeV)	-1.84 ± 0.13	-1.05 ± 0.19	-1.35 ± 0.26
$N(B^0 \to DK\pi)$	3125 ± 79	418 ± 27	185 ± 21
$N(B_s^0 \to DK\pi)$	146 ± 27	1014 ± 41	429 ± 28
$N(\mathrm{comb\ bkgd})$	5694 ± 529	2092 ± 95	1288 ± 86
$N(B \to D^{(*)}K + X)$	2648 ± 454	...	...
$N(B^0 \to D^*K\pi)$	3028 ± 115	543 ± 48	183 ± 33
$N(B_s^0 \to D^*K\pi)$	...	1493 ± 77	639 ± 52
$N(B^0 \to D^{(*)}\pi\pi)$	783 ± 67	146 ± 17	72 ± 11
$N(\Lambda_b^0 \to D^{(*)}p\pi)$	...	241 ± 47	118 ± 26
$N(\Lambda_b^0 \to D^{(*)}pK)$	416 ± 64	34 ± 9	17 ± 5
$N(B^0 \to D^{(*)}KK)$	371 ± 51	64 ± 15	33 ± 8
$N(B_s^0 \to D^{(*)}KK)$	171 ± 47	25 ± 11	14 ± 6
f^1_{signal}	0.210 ± 0.012	0.187 ± 0.017	0.214 ± 0.029
f^2_{signal}	0.192 ± 0.008	0.186 ± 0.011	0.184 ± 0.019
f^3_{signal}	0.206 ± 0.008	0.201 ± 0.012	0.225 ± 0.019
f^4_{signal}	0.201 ± 0.007	0.215 ± 0.012	0.193 ± 0.018
$f^5_{\mathrm{signal}}{}^*$	0.190 ± 0.007	0.211 ± 0.011	0.184 ± 0.017
$f^1_{\mathrm{part\ rec\ bkgd}}$	0.214 ± 0.023	0.145 ± 0.020	0.152 ± 0.042
$f^2_{\mathrm{part\ rec\ bkgd}}$	0.214 ± 0.010	0.217 ± 0.011	0.254 ± 0.021
$f^3_{\mathrm{part\ rec\ bkgd}}$	0.215 ± 0.011	0.267 ± 0.013	0.237 ± 0.021
$f^4_{\mathrm{part\ rec\ bkgd}}$	0.193 ± 0.010	0.215 ± 0.012	0.189 ± 0.019
$f^5_{\mathrm{part\ rec\ bkgd}}{}^*$	0.164 ± 0.009	0.156 ± 0.010	0.169 ± 0.018
$f^1_{\mathrm{comb\ bkgd}}$	0.870 ± 0.013	0.849 ± 0.012	0.828 ± 0.018
$f^2_{\mathrm{comb\ bkgd}}$	0.094 ± 0.008	0.092 ± 0.009	0.116 ± 0.014
$f^3_{\mathrm{comb\ bkgd}}$	0.025 ± 0.004	0.043 ± 0.007	0.027 ± 0.008
$f^4_{\mathrm{comb\ bkgd}}$	0.009 ± 0.003	0.017 ± 0.005	0.019 ± 0.007
$f^5_{\mathrm{comb\ bkgd}}{}^*$	0.002 ± 0.002	0.000 ± 0.000	0.010 ± 0.006

V_{cb} amplitudes, while the coefficients for $K^-\pi^+$ resonances are parametrized by Eq. (2). The results are

$$x_+(B_s^0 \to D\bar{K}^*(892)^0) = 0.05 \pm 0.05,$$
$$y_+(B_s^0 \to D\bar{K}^*(892)^0) = -0.08 \pm 0.11,$$
$$x_-(B_s^0 \to D\bar{K}^*(892)^0) = 0.01 \pm 0.05,$$
$$y_-(B_s^0 \to D\bar{K}^*(892)^0) = -0.08 \pm 0.12,$$

where the uncertainties are statistical only. No significant CP violation effect is observed, consistent with the expectation that V_{ub} amplitudes are highly suppressed in this control channel.

VI. SYSTEMATIC UNCERTAINTIES

Sources of systematic uncertainty on the $x_\pm$ and $y_\pm$ parameters can be divided into two categories: experimental and model uncertainties. These are summarized in Tables V and VI. The former category includes effects due to knowledge of the signal and background yields in the signal region (denoted "$\mathcal{S}/\mathcal{B}$" in Table V), the variation of

TABLE V. Experimental systematic uncertainties.

	Uncertainty							
Parameter	$\mathcal{S}/\mathcal{B}$	ϵ	$\mathcal{B}$ DP	Fit bias	$\mathcal{B}$ asym.	$\mathcal{B}$ DP asym.	ϵ asym.	Total
x_+	0.010	0.035	0.046	0.021	0.007	0.049	0.000	0.079
x_-	0.026	0.028	0.063	0.019	0.010	0.045	0.001	0.089
y_+	0.019	0.042	0.122	0.066	0.017	0.027	0.000	0.149
y_-	0.024	0.022	0.054	0.035	0.018	0.071	0.000	0.103

TABLE VI. Model uncertainties.

	Uncertainty					
Parameter	Fixed parameters	Add/rem.	Alternative model	D_s^{**} CPV	$K\pi_{\mathrm{S-wave}}$ CPV	Total
x_+	0.027	0.028	0.068	0.008	0.003	0.079
x_-	0.030	0.034	0.076	0.056	0.022	0.107
y_+	0.075	0.061	0.131	0.012	0.047	0.170
y_-	0.040	0.066	0.255	0.286	0.064	0.396

the efficiency (ϵ) across the Dalitz plot, the background Dalitz plot distributions ($\mathcal{B}$ DP) and fit bias, all of which are evaluated in similar ways to those described in Ref. [27]. Additionally, effects that may induce fake asymmetries, including asymmetry between $\bar{B}^0$ and B^0 candidates in the background yields ($\mathcal{B}$ asym.) as well as asymmetries in the background Dalitz plot distributions ($\mathcal{B}$ DP asym.) and in the efficiency variation (ϵ asym.) are accounted for. The largest source of uncertainty in this category arises from lack of knowledge of the DP distribution for the $B_s^0 \to D^* K^- \pi^+$ background.

Model uncertainties arise due to fixing parameters in the amplitude model (denoted "fixed pars" in Table VI), the addition or removal of marginal components, namely the $K^*(1410)^0$, $K^*(1680)^0$, $D_1^*(2760)^-$, $D_3^*(2760)^-$, and $D_{s2}^*(2573)^+$ resonances, in the Dalitz plot fit (add/rem.), and the use of alternative models for the $K^+\pi^-$ S-wave and $D\pi^-$ nonresonant amplitudes (alt. mod.); all of these are evaluated as in Ref. [27]. The possibilities of CP violation associated with the $D_{s1}^*(2700)^+$ amplitude (D_s^{**} CPV), and of independent CP violation parameters in the two components of the $K^+\pi^-$ S-wave amplitude [50] ($K\pi_{\mathrm{S-wave}}$ CPV), are also accounted for. The largest source of uncertainty in this category arises from changing the description of the $K^+\pi^-$ S-wave. Other possible sources of systematic uncertainty, such as production asymmetry [51] or CP violation in the $D \to K^+K^-$ and $\pi^+\pi^-$ decays [52–54], are found to be negligible.

The total uncertainties are obtained by combining all sources in quadrature. The leading sources of systematic uncertainty are expected to be reducible with larger data samples.

VII. RESULTS AND SUMMARY

The DPs for candidates in the B candidate mass signal region in the $D \to K^+K^-$ and $\pi^+\pi^-$ samples are shown separately for $\bar{B}^0$ and B^0 candidates in Fig. 7. Projections of the fit results onto $m(D\pi)$, $m(K\pi)$, and $m(DK)$ for the

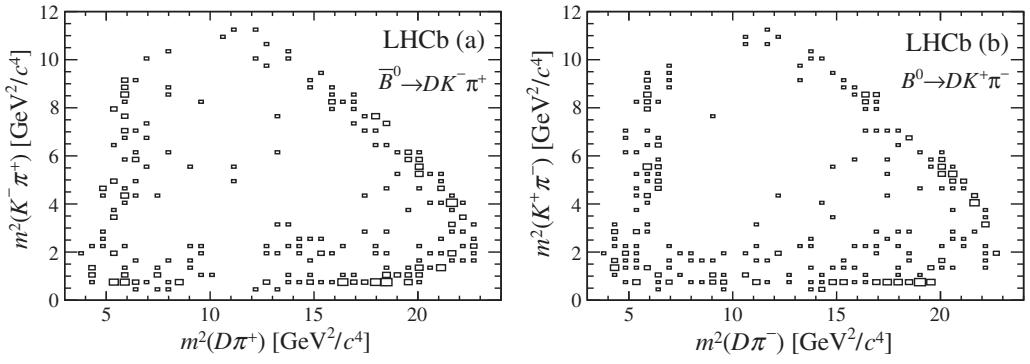

FIG. 7. Dalitz plots for candidates in the B candidate mass signal region in the $D \to K^+K^-$ and $\pi^+\pi^-$ samples for (a) $\bar{B}^0$ and (b) B^0 candidates. Only candidates in the three purest NN bins are included. Background has not been subtracted, and therefore some contribution from $\bar{B}_s^0 \to D^{*0}K^+\pi^-$ decays is expected at low $m(DK^+)$ (i.e. along the top right diagonal).

$D \to K^+K^-$ and $\pi^+\pi^-$ samples are shown separately for $\bar{B}^0$ and B^0 candidates in Fig. 8. No significant *CP* violation effect is seen.

The results, with statistical uncertainties only, for the complex coefficients c_j are given in Table VII. Due to the changes in the selection requirements, the overlap between the $D \to K^+\pi^-$ sample and the data set used in Ref. [27] is only around 60%, and the results are found to be consistent.

The results for the *CP* violation parameters associated with the $B^0 \to DK^*(892)^0$ decay are

$$x_+ = 0.04 \pm 0.16 \pm 0.11,$$
$$y_+ = -0.47 \pm 0.28 \pm 0.22,$$
$$x_- = -0.02 \pm 0.13 \pm 0.14,$$
$$y_- = -0.35 \pm 0.26 \pm 0.41,$$

where the uncertainties are statistical and systematic. The statistical and systematic correlation matrices are given in Table VIII. The results for (x_+, y_+) and (x_-, y_-) are shown as contours in Fig. 9.

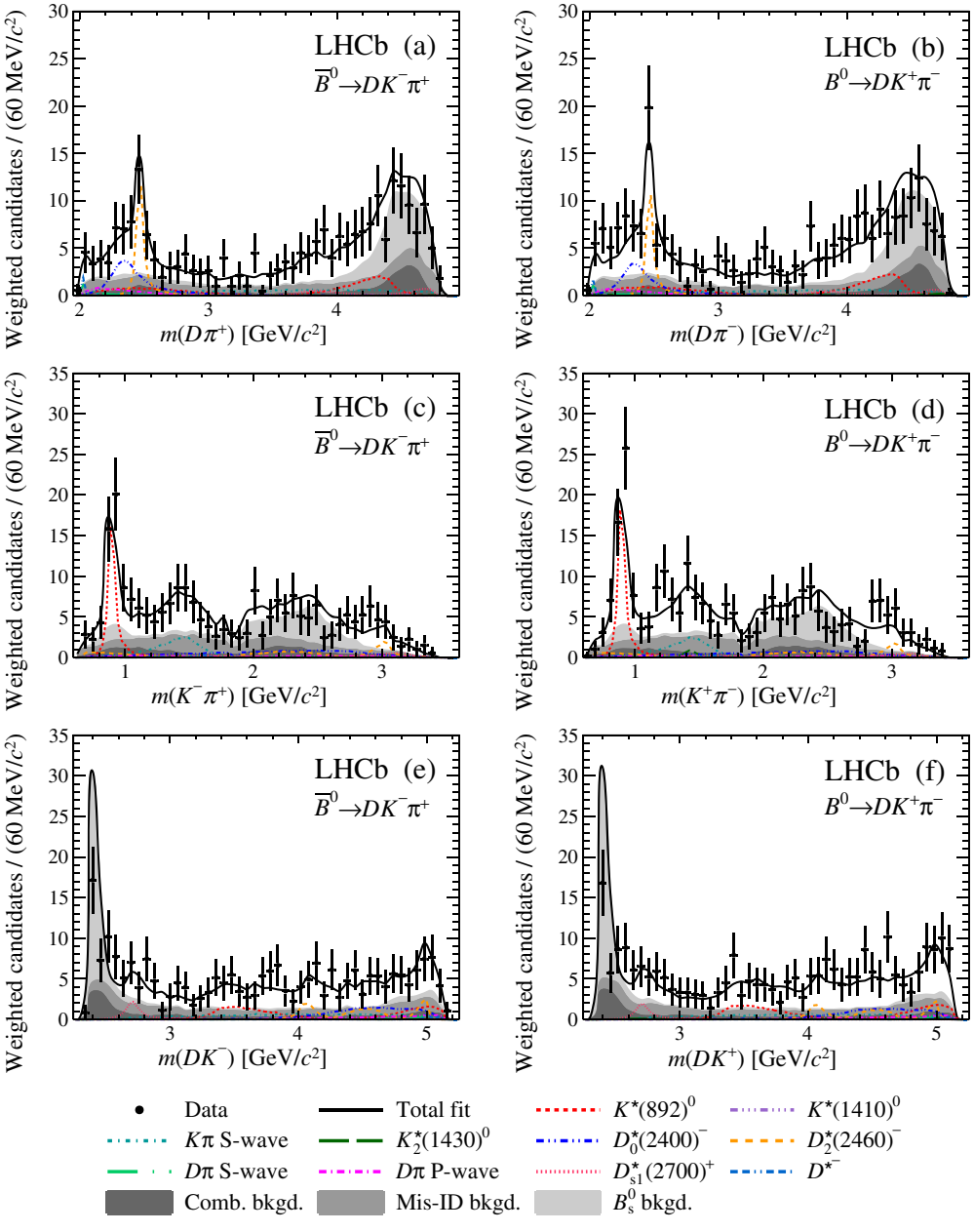

FIG. 8. Projections of the $D \to K^+K^-$ and $\pi^+\pi^-$ samples and the fit result onto (a),(b) $m(D\pi^\mp)$, (c),(d) $m(K^\pm\pi^\mp)$, and (e),(f) $m(DK^\pm)$ for (a),(c),(e) $\bar{B}^0$ and (b),(d),(f) B^0 candidates. The data and the fit results in each NN output bin have been weighted according to $\mathcal{S}/(\mathcal{S}+\mathcal{B})$ and combined. The components are described in the legend.

TABLE VII. Results for the complex coefficients c_j from the fit to data. Uncertainties are statistical only. All reported quantities are unconstrained in the fit, except that the $D_2^*(2460)^-$ component is fixed as a reference amplitude, and the magnitude of the $D_{s1}^*(2700)^+$ component is constrained. The $K^+\pi^-$ S-wave is the coherent sum of the $K_0^*(1430)^0$ and the nonresonant $K\pi$ S-wave component [50].

Resonance	Real part	Imaginary part
$K^*(892)^0$	-0.07 ± 0.10	-1.19 ± 0.04
$K^*(1410)^0$	0.16 ± 0.04	0.21 ± 0.06
$K_0^*(1430)^0$	0.40 ± 0.08	0.67 ± 0.06
Nonresonant $K\pi$ S-wave	0.37 ± 0.07	0.69 ± 0.07
$K_2^*(1430)^0$	-0.01 ± 0.06	-0.48 ± 0.04
$D_0^*(2400)^-$	-1.10 ± 0.05	-0.18 ± 0.07
$D_2^*(2460)^-$	1.00	0.00
Nonresonant $D\pi$ S-wave	-0.44 ± 0.06	0.02 ± 0.07
Nonresonant $D\pi$ P-wave	-0.61 ± 0.05	-0.08 ± 0.06
$D_{s1}^*(2700)^+$	0.57 ± 0.05	-0.09 ± 0.19

The GammaCombo package [55] is used to evaluate constraints from these results on γ and the hadronic parameters r_B and δ_B associated with the $B^0 \to DK^*(892)^0$ decay. A frequentist treatment referred to as the "plug-in" method, described in Refs. [56–59], is used. Figure 10 shows the results of likelihood scans for γ, r_B, and δ_B. Figure 11 shows the two-dimensional 68% confidence level for each pair of observables from γ, r_B, and δ_B. No value of γ is excluded at 95% confidence level (C.L.); the world-average value for γ [60,61] has a C.L. of 0.85.

The $B^0 \to DK^*(892)^0$ decay can also be used to determine parameters sensitive to γ with a quasi-two-body approach, as has been done with $D \to K^+K^-$, $\pi^+\pi^-$ [62], $K^\pm\pi^\mp$, $K^\pm\pi^\mp\pi^0$, $K^\pm\pi^\mp\pi^+\pi^-$ [62–64] and $D \to K_S^0\pi^+\pi^-$ decays [65–68]. In the quasi-two-body analysis, the results depend on the effective hadronic parameters κ, $\bar{r}_B$, and $\bar{\delta}_B$, which are, respectively, the coherence factor and the relative magnitude and strong phase of the V_{ub} and V_{cb} amplitudes averaged over the selected region of phase space [17]. Precise definitions are given in the Appendix. These parameters are calculated from the models for V_{cb} and V_{ub} amplitudes obtained from the fit for the $K^*(892)^0$ selection region $|m(K^+\pi^-) - m_{K^*(892)^0}| < 50$ MeV/c^2 and $|\cos\theta_{K^{*0}}| > 0.4$, where $m_{K^*(892)^0}$ is the known value of the $K^*(892)^0$ mass [37] and $\theta_{K^{*0}}$ is the K^{*0} helicity angle, i.e. the angle between the K^+ and D directions in the $K^+\pi^-$ rest frame. To reduce correlations with the values for r_B and δ_B determined from the DP analysis, the quantities $\bar{R}_B = \bar{r}_B/r_B$ and $\Delta\bar{\delta}_B = \bar{\delta}_B - \delta_B$ are calculated. The results are

$$\kappa = 0.958^{+0.005+0.002}_{-0.010-0.045},$$
$$\bar{R}_B = 1.02^{+0.03}_{-0.01} \pm 0.06,$$
$$\Delta\bar{\delta}_B = 0.02^{+0.03}_{-0.02} \pm 0.11,$$

where the uncertainties are statistical and systematic and are evaluated as described in the Appendix.

In summary, a data sample corresponding to 3.0 fb^{-1} of pp collisions collected with the LHCb detector has been used to measure, for the first time, parameters sensitive to the angle γ from a Dalitz plot analysis of $B^0 \to DK^+\pi^-$ decays. No significant CP violation effect is seen. The results are consistent with, and supersede, the results for $\mathcal{A}_d^{KK,\pi\pi}$ and $\mathcal{R}_d^{KK,\pi\pi}$ from Ref. [62]. Parameters that are needed to determine γ from quasi-two-body analyses of $B^0 \to DK^*(892)^0$ decays are measured. These results can be combined with current and future measurements with the $B^0 \to DK^*(892)^0$ channel to obtain stronger constraints on γ.

TABLE VIII. Correlation matrices associated with the (left) statistical and (right) systematic uncertainties of the CP violation parameters associated with the $B^0 \to DK^*(892)^0$ decay.

	x_-	y_-	x_+	y_+
x_-	1.00			
y_-	0.34	1.00		
x_+	0.10	0.05	1.00	
y_+	0.13	0.15	0.50	1.00

	x_-	y_-	x_+	y_+
x_-	1.00			
y_-	0.87	1.00		
x_+	0.25	0.29	1.00	
y_+	0.37	0.41	0.73	1.00

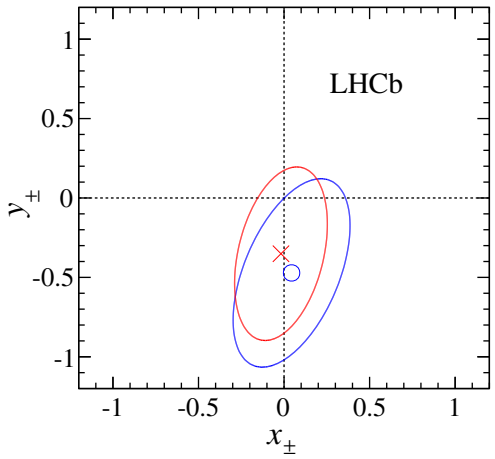

FIG. 9. Contours at 68% C.L. for the (blue) (x_+, y_+) and (red) (x_-, y_-) parameters associated with the $B^0 \to DK^*(892)^0$ decay, with statistical uncertainties only. The central values are marked by a circle and a cross, respectively.

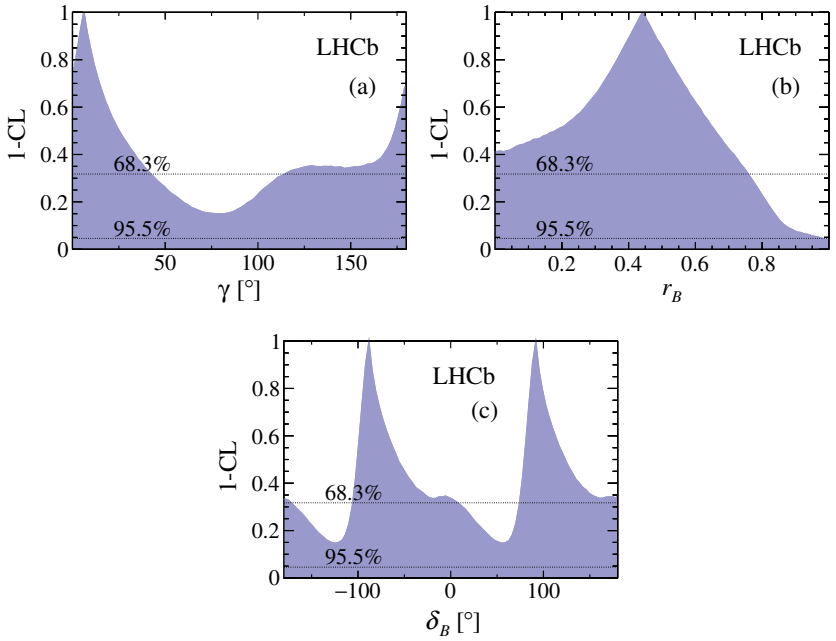

FIG. 10. Results of likelihood scans for (a) γ, (b) r_B, and (c) δ_B.

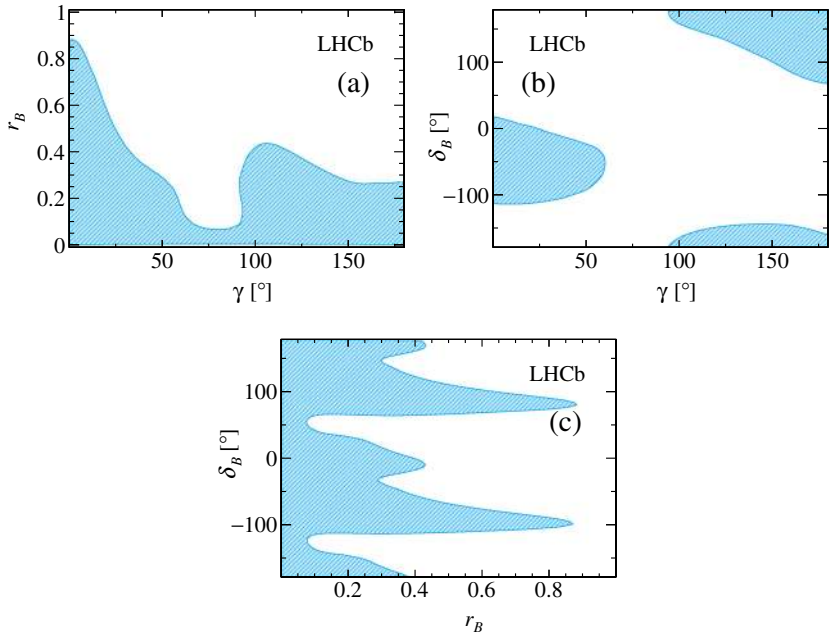

FIG. 11. Confidence level contours for (a) γ and r_B, (b) γ and δ_B, and (c) r_B and δ_B. The shaded regions are allowed at 68% C.L.

ACKNOWLEDGMENTS

We express our gratitude to our colleagues in the CERN accelerator departments for the excellent performance of the LHC. We thank the technical and administrative staff at the LHCb institutes. We acknowledge support from CERN and from the national agencies: CAPES, CNPq, FAPERJ and FINEP (Brazil); NSFC (China); CNRS/IN2P3 (France); BMBF, DFG and MPG (Germany); INFN (Italy); FOM and NWO (The Netherlands); MNiSW and NCN (Poland); MEN/IFA (Romania); MinES and FANO (Russia); MinECo (Spain); SNSF and SER (Switzerland); NASU (Ukraine); STFC (United Kingdom); NSF (USA). We acknowledge the computing resources that are provided by CERN, IN2P3 (France), KIT and DESY (Germany), INFN (Italy), SURF (The Netherlands), PIC (Spain), GridPP (United Kingdom), RRCKI and Yandex LLC (Russia), CSCS (Switzerland), IFIN-HH (Romania), CBPF (Brazil), PL-GRID (Poland) and OSC (USA). We

are indebted to the communities behind the multiple open source software packages on which we depend. Individual groups or members have received support from AvH Foundation (Germany), EPLANET, Marie Skłodowska-Curie Actions and ERC (European Union), Conseil Général de Haute-Savoie, Labex ENIGMASS and OCEVU, Région Auvergne (France), RFBR and Yandex LLC (Russia), GVA, XuntaGal and GENCAT (Spain), The Royal Society, Royal Commission for the Exhibition of 1851 and the Leverhulme Trust (United Kingdom).

APPENDIX: QUASI-TWO-BODY PARAMETERS

In the quasi-two-body analyses of $B^0 \to DK^*(892)^0$ decays, the following parameters are defined [17]:

$$\kappa = \left| \frac{\int |A_{cb}(p) A_{ub}(p)| \exp\left[i\delta(p)\right] \mathrm{d}p}{\sqrt{\int |A_{cb}(p)|^2 \mathrm{d}p \int |A_{ub}(p)|^2 \mathrm{d}p}} \right|, \tag{A1}$$

$$\bar{r}_B = \sqrt{\frac{\int |A_{ub}(p)|^2 \mathrm{d}p}{\int |A_{cb}(p)|^2 \mathrm{d}p}}, \tag{A2}$$

$$\bar{\delta}_B = \arg\left(\frac{\int |A_{cb}(p) A_{ub}(p)| \exp\left[i\delta(p)\right] \mathrm{d}p}{\sqrt{\int |A_{cb}(p)|^2 \mathrm{d}p \int |A_{ub}(p)|^2 \mathrm{d}p}} \right), \tag{A3}$$

where all the integrations are over the part of the phase space p inside the used $K^*(892)^0$ selection window. In these equations, $|A_{cb}(p)|$ and $|A_{ub}(p)|$ refer to the magnitudes of the total V_{cb} and V_{ub} amplitudes, and $\delta(p)$ is their relative strong phase. In terms of the parameters used in this analysis,

$$|A_{cb}(p)| = \left| \sum_j c_j F_j(p) \right|, \tag{A4}$$

$$|A_{ub}(p)| = \left| \sum_j c_j r_{B,j} \exp[i\delta_{B,j}] F_j(p) \right|, \tag{A5}$$

$$\delta(p) = \arg\left(\frac{\sum_j c_j r_{B,j} \exp\left[i\delta_{B,j}\right] F_j(p)}{\sum_j c_j F_j(p)} \right), \tag{A6}$$

where the $r_{B,j}$, $\delta_{B,j}$ values are allowed to differ for each $K^+\pi^-$ resonance, and $r_{B,j} = 0$ for $D\pi^-$ resonances. [The r_B, δ_B notation without the j subscript is retained for the parameters associated with the $B^0 \to DK^*(892)^0$ decay.] In the limit that there is no amplitude (either resonant or nonresonant) contributing within the $K^*(892)^0$ selection window other than those associated with the $B^0 \to DK^*(892)^0$ decay, one finds $|A_{ub}(p)| \to r_B |A_{cb}(p)|$ and $\delta(p) \to \delta_B$, and hence $\kappa \to 1$, $\bar{r}_B \to r_B$, and $\bar{\delta}_B \to \delta_B$. In order to reduce correlations between $\bar{r}_B$ and r_B and between $\bar{\delta}_B$ and δ_B, it is convenient to introduce the parameters

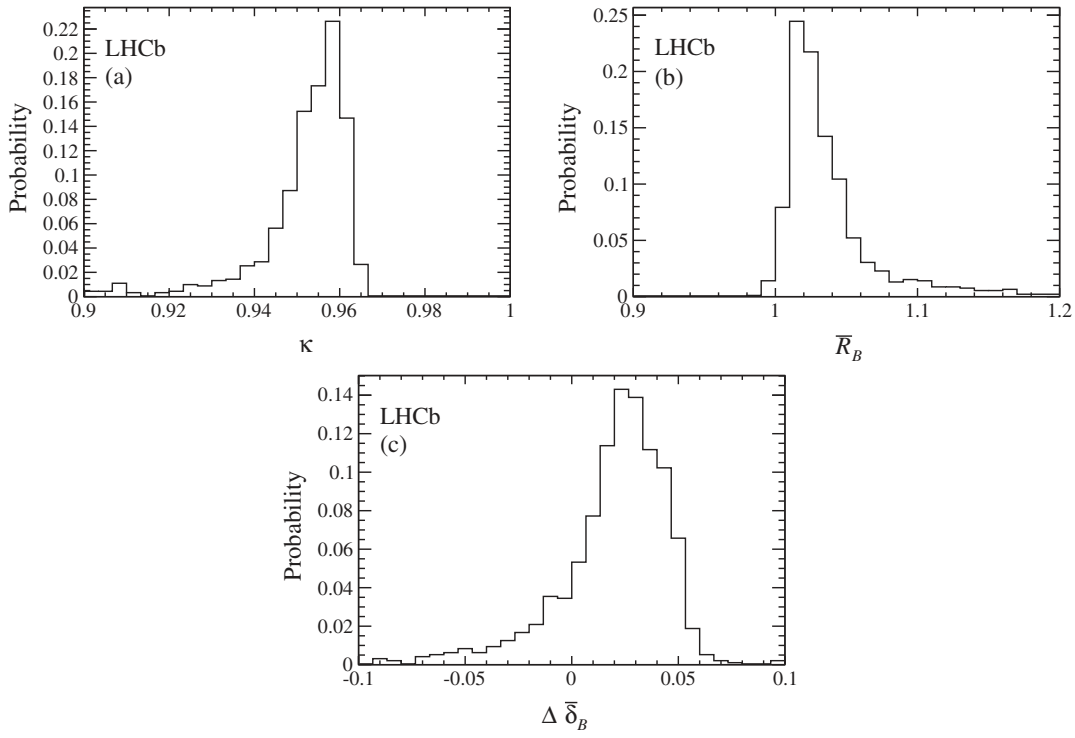

FIG. 12. Distributions of (a) κ, (b) $\bar{R}_B$, and (c) $\Delta\bar{\delta}_B$, obtained as described in the text.

$$\bar{R}_B = \frac{\bar{r}_B}{r_B}, \tag{A7}$$

$$\Delta\bar{\delta}_B = \bar{\delta}_B - \delta_B, \tag{A8}$$

which are obtained by replacing all $r_{B,j}$ by $r_{B,j}/r_B$ and all $\delta_{B,j}$ by $\delta_{B,j} - \delta_B$ in Eqs. (A4)–(A6).

These quantities are determined from the results of the Dalitz plot analysis. An alternative fit is performed with $x_{\pm,j} + iy_{\pm,j}$, defined in Eq. (2), replaced by $r_{B,j}\exp[i(\delta_{B,j} \pm \gamma)]$. The results of this fit are consistent with the values for γ, r_B, and δ_B obtained from the fitted $x_\pm$ and $y_\pm$, and are used to evaluate $|A_{cb}(p)|$, $|A_{ub}(p)|$ and $\delta(p)$ at many points inside the selection window and thereby to determine κ, $\bar{R}_B$, and $\Delta\bar{\delta}_B$. The procedure is repeated many times with both V_{cb} and V_{ub} amplitude model parameters varied within their statistical uncertainties from the fit, leading to the distributions shown in Fig. 12. Since the transformations from the fitted model parameters to the quasi-two-body parameters are highly nonlinear, the reported central values correspond to the peak positions of these distributions, while positive and negative uncertainties are obtained by incrementally including the most probable values until 68% of all entries are covered.

Sources of systematic uncertainty are accounted for by evaluating their effects on the quasi-two-body parameters. The dominant sources are from the use of an alternative description of the $K^+\pi^-$ S-wave, and from changing the treatment of CP violation in the $D_{s1}^*(2700)^+$ component and the $K^+\pi^-$ S-wave. Most systematic uncertainties are symmetrized for consistency with the rest of the analysis, but asymmetric systematic uncertainties are reported on κ since this quantity is ≤ 1 by definition.

[1] N. Cabibbo, Unitary Symmetry and Leptonic Decays, Phys. Rev. Lett. **10**, 531 (1963).

[2] M. Kobayashi and T. Maskawa, CP violation in the renormalizable theory of weak interaction, Prog. Theor. Phys. **49**, 652 (1973).

[3] L. Wolfenstein, Parametrization of the Kobayashi-Maskawa Matrix, Phys. Rev. Lett. **51**, 1945 (1983).

[4] C. Jarlskog, Commutator of the Quark Mass Matrices in the Standard Electroweak Model and a Measure of Maximal CP Violation, Phys. Rev. Lett. **55**, 1039 (1985).

[5] A. J. Buras, M. E. Lautenbacher, and G. Ostermaier, Waiting for the top quark mass, $K^+ \to \pi^+\nu\bar{\nu}$, B_s^0–$\bar{B}_s^0$ mixing and CP asymmetries in B decays, Phys. Rev. D **50**, 3433 (1994).

[6] A. Riotto and M. Trodden, Recent progress in baryogenesis, Annu. Rev. Nucl. Part. Sci. **49**, 35 (1999).

[7] M. Gronau and D. London, How to determine all the angles of the unitarity triangle from $B^0 \to DK_S^0$ and $B_s^0 \to D\phi$, Phys. Lett. B **253**, 483 (1991).

[8] M. Gronau and D. Wyler, On determining a weak phase from charged B decay asymmetries, Phys. Lett. B **265**, 172 (1991).

[9] D. Atwood, I. Dunietz, and A. Soni, Enhanced CP Violation with $B \to KD^0(\bar{D}^0)$ Modes and Extraction of the Cabibbo-Kobayashi-Maskawa Angle γ, Phys. Rev. Lett. **78**, 3257 (1997).

[10] D. Atwood, I. Dunietz, and A. Soni, Improved methods for observing CP violation in $B^\pm \to K^\pm D$ and measuring the CKM phase γ, Phys. Rev. D **63**, 036005 (2001).

[11] J. Brod and J. Zupan, The ultimate theoretical error on γ from $B \to DK$ decays, J. High Energy Phys. 01 (2014) 051.

[12] T. Gershon, On the measurement of the unitarity triangle angle γ from $B^0 \to DK^{*0}$ decays, Phys. Rev. D **79**, 051301 (2009).

[13] T. Gershon and M. Williams, Prospects for the measurement of the unitarity triangle angle γ from $B^0 \to DK^+\pi^-$ decays, Phys. Rev. D **80**, 092002 (2009).

[14] R. H. Dalitz, On the analysis of τ-meson data and the nature of the τ-meson, Philos. Mag. Ser. 5 **44**, 1068 (1953).

[15] I. I. Bigi and A. I. Sanda, On direct CP violation in $B \to \overset{(-)}{D}{}^0 K\pi$'s versus $\bar{B} \to \overset{(-)}{D}{}^0 \bar{K}\pi$'s decays, Phys. Lett. B **211**, 213 (1988).

[16] I. Dunietz, CP violation with self-tagging B^0 modes, Phys. Lett. B **270**, 75 (1991).

[17] M. Gronau, Improving bounds on γ in $B^\pm \to DK^\pm$ and $B^{\pm,0} \to DX_s^{\pm,0}$, Phys. Lett. B **557**, 198 (2003).

[18] A. A. Alves, Jr. *et al.* (LHCb Collaboration), The LHCb detector at the LHC, J. Instrum. **3**, S08005 (2008).

[19] R. Aaij *et al.* (LHCb Collaboration), LHCb detector performance, Int. J. Mod. Phys. A **30**, 1530022 (2015).

[20] A. Puig, CERN Report No. LHCb-PUB-2014-046, 2014.

[21] T. Sjöstrand, S. Mrenna, and P. Skands, A brief introduction to PYTHIA 8.1, Comput. Phys. Commun. **178**, 852 (2008); PYTHIA 6.4 physics and manual, J. High Energy Phys. 05 (2006) 026.

[22] I. Belyaev *et al.*, Handling of the generation of primary events in Gauss, the LHCb simulation framework, J. Phys. Conf. Ser. **331**, 032047 (2011).

[23] D. J. Lange, The EvtGen particle decay simulation package, Nucl. Instrum. Methods Phys. Res., Sect. A **462**, 152 (2001).

[24] P. Golonka and Z. Was, PHOTOS Monte Carlo: A precision tool for QED corrections in Z and W decays, Eur. Phys. J. C **45**, 97 (2006).

[25] J. Allison *et al.* (Geant4 Collaboration), Geant4 developments and applications, IEEE Trans. Nucl. Sci. **53**, 270 (2006); S. Agostinelli *et al.* (Geant4 Collaboration), Geant4: A simulation toolkit, Nucl. Instrum. Methods Phys. Res., Sect. A **506**, 250 (2003).

[26] M. Clemencic, G. Corti, S. Easo, C. R. Jones, S. Miglioranzi, M. Pappagallo, and P. Robbe, The LHCb simulation application, Gauss: Design, evolution and experience, J. Phys. Conf. Ser. **331**, 032023 (2011).

[27] R. Aaij *et al.* (LHCb Collaboration), Amplitude analysis of $B^0 \to \bar{D}^0 K^+ \pi^-$ decays, Phys. Rev. D **92**, 012012 (2015).

[28] R. Aaij *et al.* (LHCb Collaboration), Observation of the decay $B_s^0 \to \bar{D}^0 \phi$, Phys. Lett. B **727**, 403 (2013).

[29] R. Aaij *et al.* (LHCb Collaboration), Observation of B_s^0–$\bar{B}_s^0$ mixing and measurement of mixing frequencies using semileptonic B decays, Eur. Phys. J. C **73**, 2655 (2013).

[30] R. Aaij *et al.* (LHCb Collaboration), First evidence for the annihilation decay mode $B^+ \to D_s^+ \phi$, J. High Energy Phys. 02 (2013) 043.

[31] R. Aaij *et al.* (LHCb Collaboration), First observations of $\bar{B}_s^0 \to D^+ D^-$, $D_s^+ D^-$ and $D^0 \bar{D}^0$ decays, Phys. Rev. D **87**, 092007 (2013).

[32] M. Feindt and U. Kerzel, The NeuroBayes neural network package, Nucl. Instrum. Methods Phys. Res., Sect. A **559**, 190 (2006).

[33] M. Pivk and F. R. Le Diberder, sPlot: A statistical tool to unfold data distributions, Nucl. Instrum. Methods Phys. Res., Sect. A **555**, 356 (2005).

[34] R. Aaij *et al.* (LHCb Collaboration), Search for the decay $B_s^0 \to \bar{D}^0 f_0(980)$, J. High Energy Phys. 08 (2015) 005.

[35] R. Aaij *et al.* (LHCb Collaboration), First observation of the rare $B^+ \to D^+ K^+ \pi^-$ decay, Phys. Rev. D **93**, 051101(R) (2016).

[36] T. Skwarnicki, Ph.D. thesis, Institute of Nuclear Physics, Krakow, 1986; DESY Report No. DESY-F31-86-02, 1986.

[37] K. A. Olive *et al.* (Particle Data Group), Review of particle physics, Chin. Phys. C **38**, 090001 (2014), and 2015 update.

[38] R. Aaij *et al.* (LHCb Collaboration), Observation of overlapping spin-1 and spin-3 $\bar{D}^0 K^-$ resonances at mass 2.86 GeV/c^2, Phys. Rev. Lett. **113**, 162001 (2014).

[39] R. Aaij *et al.* (LHCb Collaboration), Dalitz plot analysis of $B_s^0 \to \bar{D}^0 K^- \pi^+$ decays, Phys. Rev. D **90**, 072003 (2014).

[40] R. Aaij *et al.* (LHCb Collaboration), Dalitz plot analysis of $B^0 \to \bar{D}^0 \pi^+ \pi^-$ decays, Phys. Rev. D **92**, 032002 (2015).

[41] A. Kuzmin *et al.* (Belle Collaboration), Study of $\bar{B}^0 \to D^0 \pi^+ \pi^-$ decays, Phys. Rev. D **76**, 012006 (2007).

[42] K. Abe *et al.* (Belle Collaboration), Study of $B^0 \to \bar{D}^{(*)0} \pi^+ \pi^-$ decays, arXiv:hep-ex/0412072.

[43] R. Aaij *et al.* (LHCb Collaboration), Observation of $B^0 \to \bar{D}^0 K^+ K^-$ and Evidence for $B_s^0 \to \bar{D}^0 K^+ K^-$, Phys. Rev. Lett. **109**, 131801 (2012).

[44] R. Aaij *et al.* (LHCb Collaboration), Study of beauty baryon decays to $D^0 p h^-$ and $\Lambda_c^+ h^-$ final states, Phys. Rev. D **89**, 032001 (2014).

[45] M. Adinolfi *et al.*, Performance of the LHCb RICH detector at the LHC, Eur. Phys. J. C **73**, 2431 (2013).

[46] E. Ben-Haim, R. Brun, B. Echenard, and T. E. Latham, JFIT: A framework to obtain combined experimental results through joint fits, arXiv:1409.5080.

[47] Laura + + Dalitz plot fitting package, http://laura.hepforge.org/, University of Warwick.

[48] R. Aaij *et al.* (LHCb Collaboration), Study of D_J meson decays to $D^+ \pi^-$, $D^0 \pi^+$ and $D^{*+} \pi^-$ final states in pp collisions, J. High Energy Phys. 09 (2013) 145.

[49] J. P. Lees *et al.* (*BABAR* Collaboration), Dalitz plot analyses of $B^0 \to D^- D^0 K^+$ and $B^+ \to \bar{D}^0 D^0 K^+$ decays, Phys. Rev. D **91**, 052002 (2015).

[50] D. Aston *et al.* (LASS Collaboration), A study of $K^- \pi^+$ scattering in the reaction $K^- p \to K^- \pi^+ n$ at 11 GeV/c, Nucl. Phys. **B296**, 493 (1988).

[51] R. Aaij *et al.* (LHCb Collaboration), Measurement of the $\bar{B}^0$–B^0 and $\bar{B}_s^0$–B_s^0 production asymmetries in pp collisions at $\sqrt{s} = 7$ TeV, Phys. Lett. B **739**, 218 (2014).

[52] Y. Amhis *et al.* (Heavy Flavor Averaging Group), Averages of b-hadron, c-hadron, and τ-lepton properties as of summer 2014, arXiv:1412.7515, updated results and plots available at http://www.slac.stanford.edu/xorg/hfag/.

[53] R. Aaij *et al.* (LHCb Collaboration), Measurement of indirect CP asymmetries in $D^0 \to K^- K^+$ and $D^0 \to \pi^- \pi^+$ decays, J. High Energy Phys. 04 (2015) 043.

[54] R. Aaij *et al.* (LHCb Collaboration), Measurement of the difference of time-integrated CP asymmetries in $D^0 \to K^- K^+$ and $D^0 \to \pi^- \pi^+$ decays, Phys. Rev. Lett. **116**, 191601 (2016).

[55] GammaCombo framework for combinations of measurements and computation of confidence intervals, http://gammacombo.hepforge.org/, CERN.

[56] R. Aaij *et al.* (LHCb Collaboration), A measurement of the CKM angle γ from a combination of $B^\pm \to D h^\pm$ analyses, Phys. Lett. B **726**, 151 (2013).

[57] LHCb Collaboration, Report No. LHCb-CONF-2014-004, 2014.

[58] LHCb Collaboration, CERN Report No. LHCb-CONF-2016-001, 2016.

[59] B. Sen, M. Walker, and M. Woodroofe, On the unified method with nuisance parameters, Statistica Sinica **19**, 301 (2009).

[60] J. Charles, A. Höcker, H. Lacker, S. Laplace, F. R. Le Diberder, J. Malclés, J. Ocariz, M. Pivk, and L. Roos (CKMfitter Group), CP violation and the CKM matrix: Assessing the impact of the asymmetric B factories, Eur. Phys. J. C **41**, 1 (2005).

[61] M. Bona *et al.* (UTfit Collaboration), The 2004 UTfit Collaboration report on the status of the unitarity triangle in the standard model, J. High Energy Phys. 07 (2005) 028.

[62] R. Aaij *et al.* (LHCb Collaboration), Measurement of CP violation parameters in $B^0 \to D K^{*0}$ decays, Phys. Rev. D **90**, 112002 (2014).

[63] B. Aubert *et al.* (*BABAR* Collaboration), Search for $b \to u$ transitions in $B^0 \to D^0 K^{*0}$ decays, Phys. Rev. D **80**, 031102 (2009).

[64] K. Negishi *et al.* (Belle Collaboration), Search for the decay $B^0 \to D K^{*0}$ followed by $D \to K^- \pi^+$, Phys. Rev. D **86**, 011101 (2012).

[65] B. Aubert *et al.* (*BABAR* Collaboration), Constraints on the CKM angle γ in $B^0 \to \bar{D}^0 K^{*0}$ and $B^0 \to D^0 K^{*0}$ from a Dalitz analysis of D^0 and $\bar{D}^0$ decays to $K_S^0 \pi^+ \pi^-$, Phys. Rev. D **79**, 072003 (2009).

[66] K. Negishi *et al.* (Belle Collaboration), First model-independent Dalitz analysis of $B^0 \to D K^{*0}$, $D \to K_S^0 \pi^+ \pi^-$ decay, Prog. Theor. Exp. Phys. **2016**, 043C01 (2016).

[67] R. Aaij *et al.* (LHCb Collaboration), Model-independent measurement of the CKM angle γ using $B^0 \to DK^{*0}$ decays with $D \to K^0_S\pi^+\pi^-$ and $K^0_S K^+K^-$, arXiv:1604.01525.

[68] R. Aaij *et al.* (LHCb Collaboration), Measurement of the CKM angle γ using $B^0 \to DK^{*0}$ with $D \to K^0_S\pi^+\pi^-$ decays, arXiv:1605.01082.

R. Aaij,[39] C. Abellán Beteta,[41] B. Adeva,[38] M. Adinolfi,[47] A. Affolder,[53] Z. Ajaltouni,[5] S. Akar,[6] J. Albrecht,[10] F. Alessio,[39] M. Alexander,[52] S. Ali,[42] G. Alkhazov,[31] P. Alvarez Cartelle,[54] A. A. Alves Jr.,[58] S. Amato,[2] S. Amerio,[23] Y. Amhis,[7] L. An,[3,40] L. Anderlini,[18] G. Andreassi,[40] M. Andreotti,[17,a] J. E. Andrews,[59] R. B. Appleby,[55] O. Aquines Gutierrez,[11] F. Archilli,[39] P. d'Argent,[12] A. Artamonov,[36] M. Artuso,[60] E. Aslanides,[6] G. Auriemma,[26,b] M. Baalouch,[5] S. Bachmann,[12] J. J. Back,[49] A. Badalov,[37] C. Baesso,[61] W. Baldini,[17,39] R. J. Barlow,[55] C. Barschel,[39] S. Barsuk,[7] W. Barter,[39] V. Batozskaya,[29] V. Battista,[40] A. Bay,[40] L. Beaucourt,[4] J. Beddow,[52] F. Bedeschi,[24] I. Bediaga,[1] L. J. Bel,[42] V. Bellee,[40] N. Belloli,[21,c] I. Belyaev,[32] E. Ben-Haim,[8] G. Bencivenni,[19] S. Benson,[39] J. Benton,[47] A. Berezhnoy,[33] R. Bernet,[41] A. Bertolin,[23] F. Betti,[15] M.-O. Bettler,[39] M. van Beuzekom,[42] S. Bifani,[46] P. Billoir,[8] T. Bird,[55] A. Birnkraut,[10] A. Bizzeti,[18,d] T. Blake,[49] F. Blanc,[40] J. Blouw,[11] S. Blusk,[60] V. Bocci,[26] A. Bondar,[35] N. Bondar,[31,39] W. Bonivento,[16] A. Borgheresi,[21,c] S. Borghi,[55] M. Borisyak,[67] M. Borsato,[38] T. J. V. Bowcock,[53] E. Bowen,[41] C. Bozzi,[17,39] S. Braun,[12] M. Britsch,[12] T. Britton,[60] J. Brodzicka,[55] N. H. Brook,[47] E. Buchanan,[47] C. Burr,[55] A. Bursche,[2] J. Buytaert,[39] S. Cadeddu,[16] R. Calabrese,[17,a] M. Calvi,[21,c] M. Calvo Gomez,[37,e] P. Campana,[19] D. Campora Perez,[39] L. Capriotti,[55] A. Carbone,[15,f] G. Carboni,[25,g] R. Cardinale,[20,h] A. Cardini,[16] P. Carniti,[21,c] L. Carson,[51] K. Carvalho Akiba,[2] G. Casse,[53] L. Cassina,[21,c] L. Castillo Garcia,[40] M. Cattaneo,[39] Ch. Cauet,[10] G. Cavallero,[20] R. Cenci,[24,i] M. Charles,[8] Ph. Charpentier,[39] M. Chefdeville,[4] S. Chen,[55] S.-F. Cheung,[56] N. Chiapolini,[41] M. Chrzaszcz,[41,27] X. Cid Vidal,[39] G. Ciezarek,[42] P. E. L. Clarke,[51] M. Clemencic,[39] H. V. Cliff,[48] J. Closier,[39] V. Coco,[39] J. Cogan,[6] E. Cogneras,[5] V. Cogoni,[16,j] L. Cojocariu,[30] G. Collazuol,[23,k] P. Collins,[39] A. Comerma-Montells,[12] A. Contu,[39] A. Cook,[47] M. Coombes,[47] S. Coquereau,[8] G. Corti,[39] M. Corvo,[17,a] B. Couturier,[39] G. A. Cowan,[51] D. C. Craik,[51] A. Crocombe,[49] M. Cruz Torres,[61] S. Cunliffe,[54] R. Currie,[54] C. D'Ambrosio,[39] E. Dall'Occo,[42] J. Dalseno,[47] P. N. Y. David,[42] A. Davis,[58] O. De Aguiar Francisco,[2] K. De Bruyn,[6] S. De Capua,[55] M. De Cian,[12] J. M. De Miranda,[1] L. De Paula,[2] P. De Simone,[19] C.-T. Dean,[52] D. Decamp,[4] M. Deckenhoff,[10] L. Del Buono,[8] N. Déléage,[4] M. Demmer,[10] D. Derkach,[67] O. Deschamps,[5] F. Dettori,[39] B. Dey,[22] A. Di Canto,[39] F. Di Ruscio,[25] H. Dijkstra,[39] S. Donleavy,[53] F. Dordei,[39] M. Dorigo,[40] A. Dosil Suárez,[38] A. Dovbnya,[44] K. Dreimanis,[53] L. Dufour,[42] G. Dujany,[55] K. Dungs,[39] P. Durante,[39] R. Dzhelyadin,[36] A. Dziurda,[27] A. Dzyuba,[31] S. Easo,[50,39] U. Egede,[54] V. Egorychev,[32] S. Eidelman,[35] S. Eisenhardt,[51] U. Eitschberger,[10] R. Ekelhof,[10] L. Eklund,[52] I. El Rifai,[5] Ch. Elsasser,[41] S. Ely,[60] S. Esen,[12] H. M. Evans,[48] T. Evans,[56] A. Falabella,[15] C. Färber,[39] N. Farley,[46] S. Farry,[53] R. Fay,[53] D. Fazzini,[21,c] D. Ferguson,[51] V. Fernandez Albor,[38] F. Ferrari,[15] F. Ferreira Rodrigues,[1] M. Ferro-Luzzi,[39] S. Filippov,[34] M. Fiore,[17,39,a] M. Fiorini,[17,a] M. Firlej,[28] C. Fitzpatrick,[40] T. Fiutowski,[28] F. Fleuret,[7,l] K. Fohl,[39] M. Fontana,[16] F. Fontanelli,[20,h] D. C. Forshaw,[60] R. Forty,[39] M. Frank,[39] C. Frei,[39] M. Frosini,[18] J. Fu,[22] E. Furfaro,[25,g] A. Gallas Torreira,[38] D. Galli,[15,f] S. Gallorini,[23] S. Gambetta,[51] M. Gandelman,[2] P. Gandini,[56] Y. Gao,[3] J. García Pardiñas,[38] J. Garra Tico,[48] L. Garrido,[37] D. Gascon,[37] C. Gaspar,[39] L. Gavardi,[10] G. Gazzoni,[5] D. Gerick,[12] E. Gersabeck,[12] M. Gersabeck,[55] T. Gershon,[49] Ph. Ghez,[4] S. Gianì,[40] V. Gibson,[48] O. G. Girard,[40] L. Giubega,[30] V. V. Gligorov,[39] C. Göbel,[61] D. Golubkov,[32] A. Golutvin,[54,39] A. Gomes,[1,m] C. Gotti,[21,c] M. Grabalosa Gándara,[5] R. Graciani Diaz,[37] L. A. Granado Cardoso,[39] E. Graugés,[37] E. Graverini,[41] G. Graziani,[18] A. Grecu,[30] P. Griffith,[46] L. Grillo,[12] O. Grünberg,[65] B. Gui,[60] E. Gushchin,[34] Yu. Guz,[36,39] T. Gys,[39] T. Hadavizadeh,[56] C. Hadjivasiliou,[60] G. Haefeli,[40] C. Haen,[39] S. C. Haines,[48] S. Hall,[54] B. Hamilton,[59] X. Han,[12] S. Hansmann-Menzemer,[12] N. Harnew,[56] S. T. Harnew,[47] J. Harrison,[55] J. He,[39] T. Head,[40] V. Heijne,[42] A. Heister,[9] K. Hennessy,[53] P. Henrard,[5] L. Henry,[8] J. A. Hernando Morata,[38] E. van Herwijnen,[39] M. Heß,[65] A. Hicheur,[2] D. Hill,[56] M. Hoballah,[5] C. Hombach,[55] L. Hongming,[40] W. Hulsbergen,[42] T. Humair,[54] M. Hushchyn,[67] N. Hussain,[56] D. Hutchcroft,[53] M. Idzik,[28] P. Ilten,[57] R. Jacobsson,[39] A. Jaeger,[12] J. Jalocha,[56] E. Jans,[42] A. Jawahery,[59] M. John,[56] D. Johnson,[39] C. R. Jones,[48] C. Joram,[39] B. Jost,[39] N. Jurik,[60] S. Kandybei,[44] W. Kanso,[6] M. Karacson,[39] T. M. Karbach,[39,†] S. Karodia,[52] M. Kecke,[12] M. Kelsey,[60] I. R. Kenyon,[46] M. Kenzie,[39] T. Ketel,[43] E. Khairullin,[67] B. Khanji,[21,39,c] C. Khurewathanakul,[40] T. Kirn,[9] S. Klaver,[55] K. Klimaszewski,[29] O. Kochebina,[7] M. Kolpin,[12] I. Komarov,[40] R. F. Koopman,[43] P. Koppenburg,[42,39] M. Kozeiha,[5] L. Kravchuk,[34] K. Kreplin,[12] M. Kreps,[49] P. Krokovny,[35] F. Kruse,[10] W. Krzemien,[29] W. Kucewicz,[27,n] M. Kucharczyk,[27]

V. Kudryavtsev,[35] A. K. Kuonen,[40] K. Kurek,[29] T. Kvaratskheliya,[32] D. Lacarrere,[39] G. Lafferty,[55,39] A. Lai,[16] D. Lambert,[51] G. Lanfranchi,[19] C. Langenbruch,[49] B. Langhans,[39] T. Latham,[49] C. Lazzeroni,[46] R. Le Gac,[6] J. van Leerdam,[42] J.-P. Lees,[4] R. Lefèvre,[5] A. Leflat,[33,39] J. Lefrançois,[7] E. Lemos Cid,[38] O. Leroy,[6] T. Lesiak,[27] B. Leverington,[12] Y. Li,[7] T. Likhomanenko,[67,66] M. Liles,[53] R. Lindner,[39] C. Linn,[39] F. Lionetto,[41] B. Liu,[16] X. Liu,[3] D. Loh,[49] I. Longstaff,[52] J. H. Lopes,[2] D. Lucchesi,[23,k] M. Lucio Martinez,[38] H. Luo,[51] A. Lupato,[23] E. Luppi,[17,a] O. Lupton,[56] A. Lusiani,[24] F. Machefert,[7] F. Maciuc,[30] O. Maev,[31] K. Maguire,[55] S. Malde,[56] A. Malinin,[66] G. Manca,[7] G. Mancinelli,[6] P. Manning,[60] A. Mapelli,[39] J. Maratas,[5] J. F. Marchand,[4] U. Marconi,[15] C. Marin Benito,[37] P. Marino,[24,39,i] J. Marks,[12] G. Martellotti,[26] M. Martin,[6] M. Martinelli,[40] D. Martinez Santos,[38] F. Martinez Vidal,[68] D. Martins Tostes,[2] L. M. Massacrier,[7] A. Massafferri,[1] R. Matev,[39] A. Mathad,[49] Z. Mathe,[39] C. Matteuzzi,[21] A. Mauri,[41] B. Maurin,[40] A. Mazurov,[46] M. McCann,[54] J. McCarthy,[46] A. McNab,[55] R. McNulty,[13] B. Meadows,[58] F. Meier,[10] M. Meissner,[12] D. Melnychuk,[29] M. Merk,[42] A Merli,[22,o] E Michielin,[23] D. A. Milanes,[64] M.-N. Minard,[4] D. S. Mitzel,[12] J. Molina Rodriguez,[61] I. A. Monroy,[64] S. Monteil,[5] M. Morandin,[23] P. Morawski,[28] A. Mordà,[6] M. J. Morello,[24,i] J. Moron,[28] A. B. Morris,[51] R. Mountain,[60] F. Muheim,[51] D. Müller,[55] J. Müller,[10] K. Müller,[41] V. Müller,[10] M. Mussini,[15] B. Muster,[40] P. Naik,[47] T. Nakada,[40] R. Nandakumar,[50] A. Nandi,[56] I. Nasteva,[2] M. Needham,[51] N. Neri,[22] S. Neubert,[12] N. Neufeld,[39] M. Neuner,[12] A. D. Nguyen,[40] C. Nguyen-Mau,[40,p] V. Niess,[5] S. Nieswand,[9] R. Niet,[10] N. Nikitin,[33] T. Nikodem,[12] A. Novoselov,[36] D. P. O'Hanlon,[49] A. Oblakowska-Mucha,[28] V. Obraztsov,[36] S. Ogilvy,[52] O. Okhrimenko,[45] R. Oldeman,[16,48,j] C. J. G. Onderwater,[69] B. Osorio Rodrigues,[1] J. M. Otalora Goicochea,[2] A. Otto,[39] P. Owen,[54] A. Oyanguren,[68] A. Palano,[14,q] F. Palombo,[22,o] M. Palutan,[19] J. Panman,[39] A. Papanestis,[50] M. Pappagallo,[52] L. L. Pappalardo,[17,a] C. Pappenheimer,[58] W. Parker,[59] C. Parkes,[55] G. Passaleva,[18] G. D. Patel,[53] M. Patel,[54] C. Patrignani,[20,h] A. Pearce,[55,50] A. Pellegrino,[42] G. Penso,[26,r] M. Pepe Altarelli,[39] S. Perazzini,[15,f] P. Perret,[5] L. Pescatore,[46] K. Petridis,[47] A. Petrolini,[20,h] M. Petruzzo,[22] E. Picatoste Olloqui,[37] B. Pietrzyk,[4] M. Pikies,[27] D. Pinci,[26] A. Pistone,[20] A. Piucci,[12] S. Playfer,[51] M. Plo Casasus,[38] T. Poikela,[39] F. Polci,[8] A. Poluektov,[49,35] I. Polyakov,[32] E. Polycarpo,[2] A. Popov,[36] D. Popov,[11,39] B. Popovici,[30] C. Potterat,[2] E. Price,[47] J. D. Price,[53] J. Prisciandaro,[38] A. Pritchard,[53] C. Prouve,[47] V. Pugatch,[45] A. Puig Navarro,[40] G. Punzi,[24,s] W. Qian,[56] R. Quagliani,[7,47] B. Rachwal,[27] J. H. Rademacker,[47] M. Rama,[24] M. Ramos Pernas,[38] M. S. Rangel,[2] I. Raniuk,[44] G. Raven,[43] F. Redi,[54] S. Reichert,[55] A. C. dos Reis,[1] V. Renaudin,[7] S. Ricciardi,[50] S. Richards,[47] M. Rihl,[39] K. Rinnert,[53,39] V. Rives Molina,[37] P. Robbe,[7,39] A. B. Rodrigues,[1] E. Rodrigues,[55] J. A. Rodriguez Lopez,[64] P. Rodriguez Perez,[55] A. Rogozhnikov,[67] S. Roiser,[39] V. Romanovsky,[36] A. Romero Vidal,[38] J. W. Ronayne,[13] M. Rotondo,[23] T. Ruf,[39] P. Ruiz Valls,[68] J. J. Saborido Silva,[38] N. Sagidova,[31] B. Saitta,[16,j] V. Salustino Guimaraes,[2] C. Sanchez Mayordomo,[68] B. Sanmartin Sedes,[38] R. Santacesaria,[26] C. Santamarina Rios,[38] M. Santimaria,[19] E. Santovetti,[25,g] A. Sarti,[19,r] C. Satriano,[26,b] A. Satta,[25] D. M. Saunders,[47] D. Savrina,[32,33] S. Schael,[9] M. Schiller,[39] H. Schindler,[39] M. Schlupp,[10] M. Schmelling,[11] T. Schmelzer,[10] B. Schmidt,[39] O. Schneider,[40] A. Schopper,[39] M. Schubiger,[40] M.-H. Schune,[7] R. Schwemmer,[39] B. Sciascia,[19] A. Sciubba,[26,r] A. Semennikov,[32] A. Sergi,[46] N. Serra,[41] J. Serrano,[6] L. Sestini,[23] P. Seyfert,[21] M. Shapkin,[36] I. Shapoval,[17,44,a] Y. Shcheglov,[31] T. Shears,[53] L. Shekhtman,[35] V. Shevchenko,[66] A. Shires,[10] B. G. Siddi,[17] R. Silva Coutinho,[41] L. Silva de Oliveira,[2] G. Simi,[23,s] M. Sirendi,[48] N. Skidmore,[47] T. Skwarnicki,[60] E. Smith,[54] I. T. Smith,[51] J. Smith,[48] M. Smith,[55] H. Snoek,[42] M. D. Sokoloff,[58,39] F. J. P. Soler,[52] F. Soomro,[40] D. Souza,[47] B. Souza De Paula,[2] B. Spaan,[10] P. Spradlin,[52] S. Sridharan,[39] F. Stagni,[39] M. Stahl,[12] S. Stahl,[39] S. Stefkova,[54] O. Steinkamp,[41] O. Stenyakin,[36] S. Stevenson,[56] S. Stoica,[30] S. Stone,[60] B. Storaci,[41] S. Stracka,[24,i] M. Straticiuc,[30] U. Straumann,[41] L. Sun,[58] W. Sutcliffe,[54] K. Swientek,[28] S. Swientek,[10] V. Syropoulos,[43] M. Szczekowski,[29] T. Szumlak,[28] S. T'Jampens,[4] A. Tayduganov,[6] T. Tekampe,[10] G. Tellarini,[17,a] F. Teubert,[39] C. Thomas,[56] E. Thomas,[39] J. van Tilburg,[42] V. Tisserand,[4] M. Tobin,[40] J. Todd,[58] S. Tolk,[43] L. Tomassetti,[17,a] D. Tonelli,[39] S. Topp-Joergensen,[56] E. Tournefier,[4] S. Tourneur,[40] K. Trabelsi,[40] M. Traill,[52] M. T. Tran,[40] M. Tresch,[41] A. Trisovic,[39] A. Tsaregorodtsev,[6] P. Tsopelas,[42] N. Tuning,[42,39] A. Ukleja,[29] A. Ustyuzhanin,[67,66] U. Uwer,[12] C. Vacca,[16,39,j] V. Vagnoni,[15] G. Valenti,[15] A. Vallier,[7] R. Vazquez Gomez,[19] P. Vazquez Regueiro,[38] C. Vázquez Sierra,[38] S. Vecchi,[17] M. van Veghel,[43] J. J. Velthuis,[47] M. Veltri,[18,t] G. Veneziano,[40] M. Vesterinen,[12] B. Viaud,[7] D. Vieira,[2] M. Vieites Diaz,[38] X. Vilasis-Cardona,[37,e] V. Volkov,[33] A. Vollhardt,[41] D. Voong,[47] A. Vorobyev,[31] V. Vorobyev,[35] C. Voß,[65] J. A. de Vries,[42] R. Waldi,[65] C. Wallace,[49] R. Wallace,[13] J. Walsh,[24] J. Wang,[60] D. R. Ward,[48] N. K. Watson,[46] D. Websdale,[54] A. Weiden,[41] M. Whitehead,[39] J. Wicht,[49] G. Wilkinson,[56,39] M. Wilkinson,[60] M. Williams,[39] M. P. Williams,[46] M. Williams,[57] T. Williams,[46] F. F. Wilson,[50] J. Wimberley,[59] J. Wishahi,[10] W. Wislicki,[29] M. Witek,[27] G. Wormser,[7] S. A. Wotton,[48] K. Wraight,[52] S. Wright,[48] K. Wyllie,[39] Y. Xie,[63] Z. Xu,[40] Z. Yang,[3] H. Yin,[63] J. Yu,[63] X. Yuan,[35] O. Yushchenko,[36]

M. Zangoli,[15] M. Zavertyaev,[11,u] L. Zhang,[3] Y. Zhang,[3] A. Zhelezov,[12] Y. Zheng,[62] A. Zhokhov,[32] L. Zhong,[3] V. Zhukov,[9] and S. Zucchelli[15]

(LHCb Collaboration)

[1]*Centro Brasileiro de Pesquisas Físicas (CBPF), Rio de Janeiro, Brazil*
[2]*Universidade Federal do Rio de Janeiro (UFRJ), Rio de Janeiro, Brazil*
[3]*Center for High Energy Physics, Tsinghua University, Beijing, China*
[4]*LAPP, Université Savoie Mont-Blanc, CNRS/IN2P3, Annecy-Le-Vieux, France*
[5]*Clermont Université, Université Blaise Pascal, CNRS/IN2P3, LPC, Clermont-Ferrand, France*
[6]*CPPM, Aix-Marseille Université, CNRS/IN2P3, Marseille, France*
[7]*LAL, Université Paris-Sud, CNRS/IN2P3, Orsay, France*
[8]*LPNHE, Université Pierre et Marie Curie, Université Paris Diderot, CNRS/IN2P3, Paris, France*
[9]*I. Physikalisches Institut, RWTH Aachen University, Aachen, Germany*
[10]*Fakultät Physik, Technische Universität Dortmund, Dortmund, Germany*
[11]*Max-Planck-Institut für Kernphysik (MPIK), Heidelberg, Germany*
[12]*Physikalisches Institut, Ruprecht-Karls-Universität Heidelberg, Heidelberg, Germany*
[13]*School of Physics, University College Dublin, Dublin, Ireland*
[14]*Sezione INFN di Bari, Bari, Italy*
[15]*Sezione INFN di Bologna, Bologna, Italy*
[16]*Sezione INFN di Cagliari, Cagliari, Italy*
[17]*Sezione INFN di Ferrara, Ferrara, Italy*
[18]*Sezione INFN di Firenze, Firenze, Italy*
[19]*Laboratori Nazionali dell'INFN di Frascati, Frascati, Italy*
[20]*Sezione INFN di Genova, Genova, Italy*
[21]*Sezione INFN di Milano Bicocca, Milano, Italy*
[22]*Sezione INFN di Milano, Milano, Italy*
[23]*Sezione INFN di Padova, Padova, Italy*
[24]*Sezione INFN di Pisa, Pisa, Italy*
[25]*Sezione INFN di Roma Tor Vergata, Roma, Italy*
[26]*Sezione INFN di Roma La Sapienza, Roma, Italy*
[27]*Henryk Niewodniczanski Institute of Nuclear Physics Polish Academy of Sciences, Kraków, Poland*
[28]*AGH—University of Science and Technology, Faculty of Physics and Applied Computer Science, Kraków, Poland*
[29]*National Center for Nuclear Research (NCBJ), Warsaw, Poland*
[30]*Horia Hulubei National Institute of Physics and Nuclear Engineering, Bucharest-Magurele, Romania*
[31]*Petersburg Nuclear Physics Institute (PNPI), Gatchina, Russia*
[32]*Institute of Theoretical and Experimental Physics (ITEP), Moscow, Russia*
[33]*Institute of Nuclear Physics, Moscow State University (SINP MSU), Moscow, Russia*
[34]*Institute for Nuclear Research of the Russian Academy of Sciences (INR RAN), Moscow, Russia*
[35]*Budker Institute of Nuclear Physics (SB RAS) and Novosibirsk State University, Novosibirsk, Russia*
[36]*Institute for High Energy Physics (IHEP), Protvino, Russia*
[37]*Universitat de Barcelona, Barcelona, Spain*
[38]*Universidad de Santiago de Compostela, Santiago de Compostela, Spain*
[39]*European Organization for Nuclear Research (CERN), Geneva, Switzerland*
[40]*Ecole Polytechnique Fédérale de Lausanne (EPFL), Lausanne, Switzerland*
[41]*Physik-Institut, Universität Zürich, Zürich, Switzerland*
[42]*Nikhef National Institute for Subatomic Physics, Amsterdam, The Netherlands*
[43]*Nikhef National Institute for Subatomic Physics and VU University Amsterdam, Amsterdam, The Netherlands*
[44]*NSC Kharkiv Institute of Physics and Technology (NSC KIPT), Kharkiv, Ukraine*
[45]*Institute for Nuclear Research of the National Academy of Sciences (KINR), Kyiv, Ukraine*
[46]*University of Birmingham, Birmingham, United Kingdom*
[47]*H.H. Wills Physics Laboratory, University of Bristol, Bristol, United Kingdom*
[48]*Cavendish Laboratory, University of Cambridge, Cambridge, United Kingdom*
[49]*Department of Physics, University of Warwick, Coventry, United Kingdom*
[50]*STFC Rutherford Appleton Laboratory, Didcot, United Kingdom*
[51]*School of Physics and Astronomy, University of Edinburgh, Edinburgh, United Kingdom*

[52]School of Physics and Astronomy, University of Glasgow, Glasgow, United Kingdom
[53]Oliver Lodge Laboratory, University of Liverpool, Liverpool, United Kingdom
[54]Imperial College London, London, United Kingdom
[55]School of Physics and Astronomy, University of Manchester, Manchester, United Kingdom
[56]Department of Physics, University of Oxford, Oxford, United Kingdom
[57]Massachusetts Institute of Technology, Cambridge, MA, United States
[58]University of Cincinnati, Cincinnati, OH, United States
[59]University of Maryland, College Park, MD, United States
[60]Syracuse University, Syracuse, NY, United States
[61]Pontifícia Universidade Católica do Rio de Janeiro (PUC-Rio), Rio de Janeiro, Brazil (associated with Institution Universidade Federal do Rio de Janeiro (UFRJ), Rio de Janeiro, Brazil)
[62]University of Chinese Academy of Sciences, Beijing, China (associated with Institution Center for High Energy Physics, Tsinghua University, Beijing, China)
[63]Institute of Particle Physics, Central China Normal University, Wuhan, Hubei, China (associated with Institution Center for High Energy Physics, Tsinghua University, Beijing, China)
[64]Departamento de Fisica, Universidad Nacional de Colombia, Bogota, Colombia (associated with Institution LPNHE, Université Pierre et Marie Curie, Université Paris Diderot, CNRS/IN2P3, Paris, France)
[65]Institut für Physik, Universität Rostock, Rostock, Germany (associated with Institution Physikalisches Institut, Ruprecht-Karls-Universität Heidelberg, Heidelberg, Germany)
[66]National Research Centre Kurchatov Institute, Moscow, Russia (associated with Institution Institute of Theoretical and Experimental Physics (ITEP), Moscow, Russia)
[67]Yandex School of Data Analysis, Moscow, Russia (associated with Institution Institute of Theoretical and Experimental Physics (ITEP), Moscow, Russia)
[68]Instituto de Fisica Corpuscular (IFIC), Universitat de Valencia-CSIC, Valencia, Spain (associated with Institution Universitat de Barcelona, Barcelona, Spain)
[69]Van Swinderen Institute, University of Groningen, Groningen, The Netherlands (associated with Institution Nikhef National Institute for Subatomic Physics, Amsterdam, The Netherlands)

[†]Deceased.
[a]Also at Università di Ferrara, Ferrara, Italy.
[b]Also at Università della Basilicata, Potenza, Italy.
[c]Also at Università di Milano Bicocca, Milano, Italy.
[d]Also at Università di Modena e Reggio Emilia, Modena, Italy.
[e]Also at LIFAELS, La Salle, Universitat Ramon Llull, Barcelona, Spain.
[f]Also at Università di Bologna, Bologna, Italy.
[g]Also at Università di Roma Tor Vergata, Roma, Italy.
[h]Also at Università di Genova, Genova, Italy.
[i]Also at Scuola Normale Superiore, Pisa, Italy.
[j]Also at Università di Cagliari, Cagliari, Italy.
[k]Also at Università di Padova, Padova, Italy.
[l]Also at Laboratoire Leprince-Ringuet, Palaiseau, France.
[m]Also at Universidade Federal do Triângulo Mineiro (UFTM), Uberaba-MG, Brazil.
[n]Also at AGH—University of Science and Technology, Faculty of Computer Science, Electronics and Telecommunications, Kraków, Poland.
[o]Also at Università degli Studi di Milano, Milano, Italy.
[p]Also at Hanoi University of Science, Hanoi, Viet Nam.
[q]Also at Università di Bari, Bari, Italy.
[r]Also at Università di Roma La Sapienza, Roma, Italy.
[s]Also at Università di Pisa, Pisa, Italy.
[t]Also at Università di Urbino, Urbino, Italy.
[u]Also at P.N. Lebedev Physical Institute, Russian Academy of Science (LPI RAS), Moscow, Russia.